Multiphoton ionization of O_2 $X\,^3\Sigma_g^-$, $a\,^1\Delta_g$, and $b\,^1\Sigma_g^+$ via the two-photon resonant $ns\sigma_g$, $nd\sigma_g$, and $nd\pi_g$ Rydberg levels

R. Ogorzalek Loo,[a] W. J. Marinelli,[b] P. L. Houston, S. Arepalli,[c] and J. R. Wiesenfeld
Department of Chemistry, Cornell University, Ithaca, New York, 14853-1301

R. W. Field
Department of Chemistry, Massachusetts Institute of Technology, Cambridge, Massachusetts 02139

(Received 1 June 1989; accepted 24 July 1989)

Multiphoton ionization spectra have been obtained and analyzed for excitation in the 215–360 nm region from the $X\,^3\Sigma_g^-$, $a\,^1\Delta_g$, and $b\,^1\Sigma_g^+$ states of O_2. The 0–0 band of the $C\,^1\Pi_g$ state is reported for the first time. Measurements of other vibrational bands terminating in the $C\,^3\Pi_g$ and $d\,^1\Pi_g$ states are in good agreement with determinations by other groups. Several vibrational levels ($v' = 0$–5) of the $3d\pi_g$ Rydberg complex have been assigned on the basis of (1) an analysis of the spin–orbit couplings between the (Λ,S) basis-set states, (2) spectral simulation, and (3) the behavior of the states when the excitation radiation is changed from linear to circular polarization.

I. INTRODUCTION

It is surprising how little is known about the Rydberg levels of even such a fundamental and practically important diatomic molecule as O_2. This is particularly true of the gerade levels, to which one-photon absorption from the ground state, $X\,^3\Sigma_g^-$, is forbidden. This paper examines in detail the $3s\sigma_g$ and $3d\pi_g$ Rydberg levels of O_2 and suggests assignments for some $4s\sigma_g$, $3d\sigma_g$, and $3d\delta_g$ levels. The $3s\sigma_g$ levels have been experimentally observed and analyzed in other studies,[1–15] but our data provide several previously unobserved bands, originating from the O_2 $^1\Delta_g$ state. The $ns\sigma_g$, $nd\sigma_g$, and $nd\pi_g$ levels, also predicted by theoretical calculations,[4,16] have been recently observed in multiphoton ionization experiments, as have the $nd\delta_g$ levels.[9,17,18] However, both theory and experiment have ignored spin–orbit coupling of the $nd\pi_g$ levels. A more plausible assignment of the $3d\pi_g$ levels is presented in this work based (1) on a calculation of spin–orbit splittings, (2) on spectral simulation, and, most importantly, (3) on the behavior of each of the bands when the two-photon excitation light is changed between linear and circular polarization.

A. Previous experimental observations of the $3s\sigma_g$ levels

An understanding of the $3s\sigma_g$ Rydberg levels has been achieved only after a long and circuitous history of experiment and calculation. Discrete features superimposed on the maximum intensity portion of the Schumann–Runge continuum were first observed in electron-impact energy-loss spectra by Schulz and Dowell,[19] and indications of this structure can be seen in the later work of Lassettre *et al.*[20] and of Geiger and Schröder.[21] These features were not generally apparent in one-photon absorption spectra, although "wiggles" in the Schumann–Runge continuum, initially attributed by Bixon, Raz, and Jortner[22] to resonances in the photodissociation of O_2, were observed in some studies using continuum light sources.[22,23] Classification of the wiggles as $3s\sigma_g$ $^3\Pi_g \leftarrow X\,^3\Sigma_g^-$ bands was not an obvious choice because of the expected zero dipole oscillator strength of the forbidden $g \leftarrow g$ transition, although the transition could be induced by electric quadrupole or magnetic dipole terms.[24,25]

Before the use of laser-based techniques, electron scattering provided most of the information about these forbidden transitions. Electron transmission measurements performed by Sanche and Schulz[1–3] indirectly exposed the O_2 $^1\Pi_g$ and $^3\Pi_g$ Rydberg states. In the 8–11 eV energy region, they identified 17 resonances which they attributed to the O_2^+ $X\,^2\Pi_g$ core. Cartwright *et al.*[4] studied electron energy loss in scattering from O_2 and reported spectra obtained at various scattering angles for an incident electron energy of 45 eV. Four vibrational levels superimposed on the Schumann–Runge continuum were readily apparent. Their accompanying theoretical calculations helped to assign these features to symmetry-forbidden transitions from the ground state of configuration

$$\cdots(\sigma_g 2p)^2(\pi_u 2p)^4(\pi_g 2p)^2 \quad X\,^3\Sigma_g^-$$

[where $\cdots$ corresponds to $(\sigma_g 1s)^2(\sigma_u 1s)^2(\sigma_g 2s)^2(\sigma_u 2s)^2$] to vibrational levels $v' = 0$–3 of the $3s\sigma_g$ $^3\Pi_g$ member having the configuration

$$\cdots(\sigma_g 2p)^2(\pi_u 2p)^4(\pi_g 2p)(3s\sigma_g) \quad C\,^3\Pi_g.$$

They determined that the C state $v = 0$ level lay at 8.145 $\pm$ 0.020 eV. Huebner *et al.*[5] confirmed these measurements using 100 eV incident electrons and determined that the $C\,^3\Pi_g$ state contributed less than 0.5% to the total oscillator strength of the Schumann–Runge continuum.

Trajmar, Cartwright, and Hall[6] subsequently reported O_2 energy-loss spectra obtained at low impact energies (0.2–

[a] Current address: P8-03, Pacific Northwest Laboratory, P.O. Box 999, Richland, Washington 99352.
[b] Current address: Physical Sciences, Inc., Research Park, Andover, MA 01810.
[c] Current address: Lockheed ESC, 2400 Nasa Road One, Houston, TX 77058.

 0021-9606/89/215185-16$02.10

7.0 eV) and high scattering angles, reconfirming the earlier identification of the $C\,^3\Pi_g$ bands and proposing that excitations to the $3s\sigma_g\,^1\Pi_g$ ($v' = 0$, 1, 2, and 3) levels contributed to energy-loss peaks at 8.595, 8.826, 9.045, and 9.27 eV, partially overlapping the $C\,^3\Pi_g$ bands. The $3s\sigma_g\,^1\Pi_g$ Rydberg state, also known as the d state, arises from the same molecular-orbital configuration as does the $C\,^3\Pi_g$ state. The 50 meV energy resolution of their experiments was insufficient to separate the new bands from the $^3\Pi_g$ bands. Instead, their assignment relied upon the characteristic behavior of optically-forbidden transitions in energy-loss experiments.[3,7,26–33] In these experiments, structure apparent under conditions of high incident energy and nonzero scattering angle support a symmetry-forbidden nature for the transition, while structure apparent under conditions of low incident energy and high scattering angle suggest a spin-forbidden nature. Since the structure atop the Schumann–Runge continuum displayed different relative intensities among its members for high- and low-incident-energy electrons, partially overlapping $^1\Pi_g$ and $^3\Pi_g$ bands were suggested. Spence[8] confirmed the diagnostic intensity behavior in further energy-loss experiments. The energies of the proposed $d\,^1\Pi_g$ bands differed from those theoretically calculated[4] by 0.1 eV.

The publication by York and Comer[7] of another relevant electron energy-loss study made it clear that the location of the $^1\Pi_g$ Rydberg levels was far from resolved, however. They reproduced the relative intensity variation attributed to the two Rydberg series, but also observed three additional spin-forbidden bands. The energies of the new transitions agreed well with those originally expected for the $d\,^1\Pi_g$ state, providing singlet–triplet splittings near the 110 meV value predicted by Cartwright *et al.*[4] and a vibrational constant, ω_e, consistent with that of the $C\,^3\Pi_g$ state. York and Comer proposed that $v' = 0$–2 of $d\,^1\Pi_g$ lay at 8.232, 8.464, and 8.686 eV, respectively, while the spin-forbidden components of Trajmar, Cartwright, and Hall[6] at 8.616, 8.843, 9.059, 9.282, 9.504, and 9.715 eV corresponded to $v' = 0$–5 of a different series, which they labeled the σ series.

Recently, several groups[9–13,34] have applied multiphoton ionization (MPI) spectroscopy to the detection of the $3s\sigma_g$ Rydberg states, thus making it possible to study one-photon forbidden, two-photon allowed excited states of O_2 with optical radiation. Sur *et al.*[10,11] have published spectra of the $3s\sigma_g\,^3\Pi_g \leftarrow\leftarrow X\,^3\Sigma_g^-$ and $3s\sigma_g\,^1\Pi_g \leftarrow\leftarrow X\,^3\Sigma_g^-$ transitions (where the $\leftarrow\leftarrow$ notation indicates the absorption of two photons), confirming the assignment by York and Comer that the C and d states lie at 8.14 and 8.228 eV, respectively. Further work by Katsumata and co-workers[13] and by Johnson, Long, and Hudgens[12] is in agreement with these results. Transitions from $O_2\,^1\Delta_g$ to the $3s\sigma_g\,^1\Pi_g$ and $^3\Pi_g$ states have also been observed by Johnson, Long, and Hudgens.

However, further confusion arose following an examination of the 1–5μ emission spectrum from the negative glow of a pulsed oxygen discharge. Barowy, Sakai, and Chang[35] observed four features at 6941.0, 6953.1, 6949.4, and 6947.1 cm^{-1} that they attributed to the $(v',v'')f\,^1\Sigma_u^+ \rightarrow d\,^1\Pi_g$ $\Delta v = 0$ sequence for $v' = v'' = 0$, 1, 2, and 3, respectively. Their assignment places $v = 0$–3 of $d\,^1\Pi_g$ at 69 321.0, 71 201.1, 73 054.9, and 74 878.2 cm^{-1} (8.595, 8.828, 9.057, and 9.283 eV) in agreement with the early assignments of Trajmar, Cartwright, and Hall[6] and of Spence,[8] but in disagreement with those of York and Comer[7] and the MPI groups.[10,12]

Recently, translational spectroscopy[15,36,37] has been used to study the dissociative charge exchange of 2–4 keV O_2^+ ions with cesium atoms. Electron capture by the O_2^+ predominantly populates $v = 0$–8 of the $O_2\,^1\Pi_g$ and $^3\Pi_g$ states, which subsequently predissociate to $O(^3P) + O(^3P)$, $O(^3P) + O(^1D)$, and, for the $^1\Pi_g$ state only, to $O(^1D) + O(^1D)$. [The spin-forbidden $O(^3P) + O(^1D)$ products observed in the $^1\Pi_g$ predissociation were attributed to spin–orbit coupling between the $^1\Pi_g$ Rydberg state and the $1\,^3\Pi_g$ valence state.] Rotational resolution has been attained for the $v = 4$ level of the $d\,^1\Pi_g$ state. The $^3\Pi_g$ assignments resulting from these studies are in agreement with all of the previous measurements,[4–8,11,12] while the $^1\Pi_g$ assignments are consistent with those of York and Comer[7] and the MPI groups.[10,12] From a comparison of these results to those of Trajmar *et al.*,[6,38] and Sanche and Schulz,[1–3] it is clear that a number of unassigned peaks from 8.9–9.8 eV in the earlier measurements are really the $v = 3$–7 vibrational bands of the $3s\sigma_g\,^1\Pi_g$ and $^3\Pi_g$ states.

B. Theoretical predictions for the $3s\sigma_g$ and $3d\pi_g$ levels

Theoretical work has also been extremely important in predicting energies, bond lengths, potentials, and Rydberg–valence interactions in the O_2 Rydberg states.[39–46] Among the earliest calculations were those of Leclercq,[40] who used a single-excitation configuration-mixing (CM) approach to compute the energy levels of the first Rydberg terms of symmetry $^3\Sigma_u^-$ and $^3\Pi_u$ converging to different states of O_2^+. In a subsequent theoretical paper, Betts and McKoy[16] performed one-electron pseudopotential calculations and obtained energies for states with $ns\sigma_g$, $np\sigma_u$, $nd\pi_g$, and $nd\sigma_g$ Rydberg orbital symmetries for $n = 3$–7, but did not distinguish between states of different overall symmetry or multiplicity arising from the same orbital configuration (e.g., Σ^+, Σ^-, and Δ from $nd\pi_g$ or $^1\Pi_g$ vs $^3\Pi_g$ from $ns\sigma_g$).[16] Nevertheless, their predictions were generally within 5%–10% of available experimental measurements of the energy relative to the ionization potential. A similar calculation, but distinguishing between different symmetries and multiplicities and using the improved virtual-orbital method, was performed by Cartwright *et al.*[4] in 1973. The improved virtual-orbital method is an approach in which the form of the Hartree–Fock Hamiltonian is modified so that the virtual orbitals are good approximations to the self-consistent excited-state orbitals. It is this type of calculation which is most often used to determine the absolute energies of the $ns\sigma_g$, $nd\sigma_g$, and $nd\pi_g$ Rydberg states.

All-valence-electron CM calculations on numerous O_2 electronic states were performed by Buenker *et al.*,[41–43] but especially relevant to this work are their studies of states with Π_g symmetry. Those studies employed flexible atomic-orbital basis sets, accounting for all single and double excita-

tions with respect to the most important configurations in a given electronic state. From those studies they concluded that the splitting between the $^1\Pi_g$ and $^3\Pi_g$ Rydberg states was on the order of 0.1 eV.

Saxon and Liu[44–46] performed *ab initio* configuration-interaction calculations on the $^3\Sigma_g^-$, $^3\Sigma_u^-$, $^3\Pi_g$, $^1\Pi_g$, and $^1\Sigma_g^+$ states of O_2. These calculations were expected to provide excellent relative placement of the states but to overestimate the term energies of the Rydberg states. They determined that the minima in both the $^3\Pi_g$ and $^1\Pi_g$ potential curves lay at 2.15 a_0 (1.14 Å), while those in the $^3\Sigma_g^-$ and $^1\Sigma_g^+$ curves lay at 2.16 a_0. In keeping with the similarity of Rydberg-state molecular constants to those of the ion, these values are only 0.02–0.03 Å smaller than the O_2^+ $X\,^2\Pi_g$ bond length of 1.1164 Å.[47]

Recently, Chung, Lin, and Lee[48] have performed Hartree–Fock calculations for O_2 Rydberg states of the symmetry $[O_2^+\ X\,^2\Pi_g(n,l)]\ ^{1,3}\Pi_{g,u}$, for (n,l) from (3,0) to (10,9). Although their frozen-core approximation works well with high-n Rydberg states, it is expected to do rather poorly with low-n Rydberg electrons which perturb the core electrons. Consequently, the 10% deviation between the calculated $3s\sigma_g\ ^3\Pi_g$ and $3s\sigma_g\ ^1\Pi_g$ energies of 9.03 and 9.05 eV at $R = 1.207$ Å and the experimental values of 8.14 and 8.223 eV is not surprising.

The present work was begun with several goals in mind. One was to further our understanding of the O_2 $3s\sigma_g$ Rydberg levels by recording as many $^3\Pi_g$ and $^1\Pi_g$ bands as possible, starting from both the O_2 $X\,^3\Sigma_g^-$ and $a\,^1\Delta_g$ states.

At the time when we obtained our first spectra[9] there were no measurements of the $nd\pi_g$ Rydberg levels. A second goal, therefore, was to observe and interpret the two-photon resonant, three-photon ionization spectra. Although we were quickly able to observe the transitions,[9] their interpretation has been more elusive. We report here 4–6 vibrational bands for each of several transitions to $3d\pi_g$ Rydberg levels from O_2 $X\,^3\Sigma_g^-$ and O_2 $a\,^1\Delta_g$ as well as one transition from O_2 $b\,^1\Sigma_g^+$. While polarization studies indicate that transitions to several of these $3d\pi_g$ levels derive their oscillator strength from the Δ or Σ character of the upper states, none of the levels can be characterized properly by a Λ–S coupling scheme. The explanation has required analysis of the spin–orbit splittings and mixings using the method described in the Appendix. During the course of our work, Park *et al.*[17,18] have reported similar spectra starting from the O_2 $X\,^3\Sigma_g^-$ state in a cooled molecular beam. Although their spectra and ours are in good agreement, we disagree over the interpretation, as discussed in Sec. IV.

A third goal in these studies was to develop a sensitive method for detection of O_2 $^1\Delta_g$, a species important in planetary atmospheres,[49–52] in chemical reactions,[53] and as an energy storage medium for chemical lasers.[54–57] O_2 $^1\Delta_g$ has been detected previously by its 1.27 μm emission to the ground state,[58] by its ultraviolet absorption,[59] and by coherent anti-Stokes Raman spectroscopy.[60] When we undertook this study,[9] detection of O_2 $^1\Delta_g$ by MPI had not been reported. Since then, however, Johnson, Long, and Hudgens[12] have successfully observed transitions from O_2 $^1\Delta_g$ to the $3s\sigma_g\ ^1\Pi_g$, $^3\Pi_g$ states, with a detection limit of 5×10^9 molecules/cm^3. In the region where our spectra overlap, the findings reported here are in good agreement with theirs. In addition, we have also detected the previously unobserved 0–0 band of the $3s\sigma_g\ ^1\Pi_g \leftarrow\leftarrow {}^1\Delta_g$ transition and have obtained evidence as well for the 4–0 and 5–0 bands of that same transition. Representative bands of $3s\sigma_g$ and $3d\pi_g$ transitions have been investigated using both linearly and circularly polarized light. Finally, possible positions and assignments for transitions from $X\,^3\Sigma_g^-$, $a\,^1\Delta_g$, and $b\,^1\Sigma_g^+$ to $3d\sigma_g$, $4s\sigma_g$, and $3d\delta_g$ Rydberg levels are discussed.

II. EXPERIMENT

Multiphoton ionization of O_2 following two-photon excitation with a tunable dye laser was performed using either a static cell or a flow cell. The static cell, which was used primarily for preliminary MPI experiments on O_2 $^3\Sigma_g^-$, was made of Pyrex tubing 10 cm long by 3.75 cm in diameter and equipped with Suprasil windows and a cold finger. Two stainless-steel electrodes separated by 1 cm were used to collect the ions. The laser light was focused between the electrodes using a 10 cm focal length lens.

The flow cell was constructed primarily for observation of MPI of O_2 $^1\Delta_g$. A diagram is shown in Fig. 1. Ultrahigh purity O_2 was admitted via a needle valve and flowed through a microwave discharge[61] at a pressure of 0.5–1.0 Torr with a linear velocity of approximately 100 cm/s. For lower concentrations of oxygen, a helium or argon carrier gas was added. An alternate flow route allowed mercuric oxide mirrors to be created downstream of the microwave discharge to act as a trap for oxygen atoms.[62–64] The absence of O atoms was checked by MPI at 226 nm on the $2p^3 3p(^3P) \leftarrow\leftarrow 2p^4(^3P)$ transitions.[65] Any ion formed in the discharge were removed with biased secondary electrodes upstream of

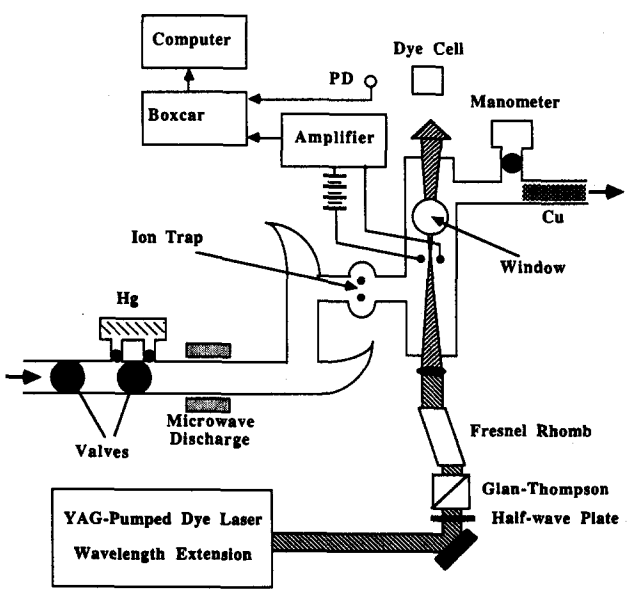

FIG. 1. Diagram of the flow cell apparatus used in these experiments. (PD denotes photodiode detector).

the observation region. The cell itself was 25.4 cm long by 5 cm in diameter and was fitted with two Suprasil windows for entrance and exit of laser light and with one Suprasil window mounted at a right angle to allow for fluorescence detection. Current created by MPI was monitored by two tungsten electrodes mounted at the center of the cell and separated by 2 cm.

The nature and origin of some of the MPI transitions were also confirmed by generating O_2 $^1\Delta_g$ by photolysis of ozone. A different flow cell was used for these experiments. It consisted of a 1 cm×1 cm cross-section quartz tube equipped with two stainless-steel electrodes separated by 1 cm. Pure ozone (100 mTorr) or ozone buffered with helium (2 Torr) was photolyzed using the 266 nm radiation from a quadrupled Nd:YAG laser (where YAG denotes yttrium aluminum garnet) (Quanta Ray, DCR-1). The O_2 $^1\Delta_g$ molecules so formed were probed after about 100 ns using radiation from the tunable dye laser system. The 266 nm radiation was either used unfocused with a 4 mm aperture or weakly focused by a 1 m focal length lens. The probe beam was focused with a 10 cm focal length lens.

The primary electrodes in the static cell and the flow cells were biased with up to 500 V and connected to a current amplifier. The amplified output was fed to a boxcar integrator to average the results of 1–10 laser pulses at each wavelength step. The boxcar output was sampled by an analog-to-digital converter connected to a laboratory computer (DEC LSI-11/2 or 11/23). Fluctuations in the intensity of the laser light were monitored continuously using a dye cell and photodiode combination, the output of which was fed to a second channel of the boxcar and stored independently in the computer. This second channel was used to normalize the spectra. For all spectra reported in this paper it was found that the ion intensity scaled as the square of the laser power.

The ionization laser was a Nd:YAG-pumped dye laser system with a provision for doubling and mixing (Quanta Ray DCR-2A or DCR-1A, PDL-1, WEX). For a few experiments, intracavity étalons were used in both the dye laser and the YAG oscillator, along with the Quanta Ray ELN-1 electronic line narrowing system, to reduce the laser bandwidth to roughly 0.1 cm^{-1} at 250 nm.

Transitions which could be observed without the microwave discharge were attributed to O_2 $X\,^3\Sigma_g^-$, while those which were observed only when the microwave discharge was "on" were attributed to either O_2 $a\,^1\Delta_g$, $b\,^1\Sigma_g^+$, or vibrationally excited $X\,^3\Sigma_g^-$. It was possible to rule out $b\,^1\Sigma_g^+$ as the initial state in some of the transitions by saturating the O_2 with water vapor, an efficient quencher for O_2 $^1\Sigma_g^+$.[66]

Further information on the identity of the excited states of oxygen was obtained from studies which compared spectra recorded with linearly and circularly polarized light at the same total intensity. For electronic transitions of the type $|\Omega \pm 1\rangle \leftarrow\leftarrow |\Omega\rangle$ or $|\Omega \pm 2\rangle \leftarrow\leftarrow |\Omega\rangle$, the intensities of all branches (*O*, *P*, *Q*, *R*, and *S*) are a factor of 3/2 stronger when excited by circularly polarized light than with linearly polarized light. This is also true of the *O*, *P*, *R*, and *S* branches of a $|\Omega\rangle \leftarrow\leftarrow |\Omega\rangle$ transition, although these branches may be difficult to observe since the *Q* branch is often dominant in such transitions. Thus, when the polarization of the exciting light is changed from linear to circular in any spectrum containing only these branch and transition combinations, the total intensity will increase, but the overall appearance of the spectrum will be unaltered. However, the *Q* branch of a $|\Omega\rangle \leftarrow\leftarrow |\Omega\rangle$ transition behaves uniquely; its intensity when observed with circularly polarized light is generally much smaller than 3/2 that observed with linearly polarized light. In some cases, the *Q* branch will vanish in circularly polarized light. The polarization behavior detailed above also applies in transitions to states of mixed character for which the oscillator strength arises from $\Delta\Omega = 0$ vs $\Delta\Omega \neq 0$ contributions. Clearly, polarization variation is a powerful tool for identifying features which derive their oscillator strength from $\Delta\Omega = 0$ transitions. Further discussions of two-photon line strengths for circularly and linearly polarized light may be found in Refs. 67–76.

III. RESULTS

Several bands of oxygen were observed via an increase in ion current as the laser was scanned through the range from roughly 215–360 nm. These bands arise from two-photon transitions to the $ns\sigma_g$, $n'd\sigma_g$, $n'd\pi_g$, and $n'd\delta_g$ Rydberg levels, where $n = 3$, 4, and 5 and $n' = 3$ and 4. Additional bands are attributed to a bound valence state.

Four series of $3s\sigma_g$ Rydberg transitions were observed. They are as follows:

$$^3\Pi_g \leftarrow\leftarrow {}^3\Sigma_g^-,$$
$$^1\Pi_g \leftarrow\leftarrow {}^3\Sigma_g^-,$$
$$^3\Pi_g \leftarrow\leftarrow {}^1\Delta_g,$$
$$^1\Pi_g \leftarrow\leftarrow {}^1\Delta_g.$$

Wavelengths and assignments for these transitions are summarized in Tables I and II. The 0–0 band of the $^1\Pi_g \leftarrow\leftarrow {}^1\Delta_g$ transition is illustrated in Fig. 2.

Representative spectra of several two-photon resonant $3d\sigma_g$, $3d\pi_g$, $3d\delta_g$, and $4s\sigma_g$ transitions are displayed in Figs. 3–7, while the wavelengths and total energies are summar-

TABLE I. Observed $3s\sigma_g$ $^3\Pi_g$ bands in the multiphoton ionization of O_2.

Lower state	Upper v'	Wavelength[a] (nm)	State energy[b] (eV)	State energy[b] (cm^{-1})
$X\,^3\Sigma_g^-$	0	304.5	8.141	65 661
$X\,^3\Sigma_g^-$	1	295.4	8.391	67 678
$X\,^3\Sigma_g^-$	2	287.8	8.612	69 462
$X\,^3\Sigma_g^-$	3	280.6	8.836	71 266
$X\,^3\Sigma_g^-$	4	274.2	9.042	72 932
$a\,^1\Delta_g$	2	325.0	8.605	69 407

[a] Not air-to-vacuum corrected.

[b] Energies are measured relative to the lowest vibrational level of the ground state and quoted based on the band center positions. Consequently, uncertainties in the state energies of several tens of cm^{-1} are expected, especially in light of the predissociation broadening prevalent in the $^3\Pi_g$ levels.

TABLE II. Observed $3s\sigma_g\ ^1\Pi_g$ bands in the multiphoton ionization of O_2.

Lower state	Upper v'	Wavelength[a] (nm)	Energy[b] (eV)	Energy[b] (cm^{-1})
$X\ ^3\Sigma_g^-$	0	301.2	8.231	66 387
$X\ ^3\Sigma_g^-$	1	293.0	8.460	68 234
$X\ ^3\Sigma_g^-$	2	285.1	8.694	70 121
$X\ ^3\Sigma_g^-$	3	277.8	8.924	71 976
$a\ ^1\Delta_g$	0	342.1[c]	8.223	66 325
$a\ ^1\Delta_g$	1	331.5[c]	8.455	68 198
$a\ ^1\Delta_g$	2	321.5[c]	8.689	70 082
$a\ ^1\Delta_g$	3	312.1[c]	8.921	71 958
$a\ ^1\Delta_g$	4	303.(?)[c]	9.16(?)[c]	73 872(?)[c]
$a\ ^1\Delta_g$	5	295.5(?)[c]	9.37(?)[c]	75 547(?)[c]

[a] Not air-to-vacuum corrected; (?) indicates tentative assignments.
[b] Energies quoted relative to the lowest vibrational level of the ground state. For excitations from the $a\ ^1\Delta_g$ state, the energies are based on the most intense peak in the spectrum, while those from $X\ ^3\Sigma_g^-$ are based on the band center. This method leads to uncertainties of 50 cm^{-1} or more, but is employed here because few of these bands have been rotationally assigned.
[c] The spectra in this region may be complicated by other states. (See Sec. IV B.)

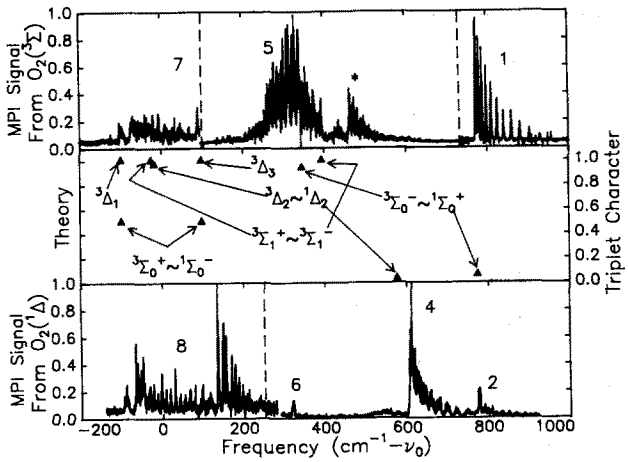

FIG. 3. The 2 + 1 MPI spectrum of the 1–0 bands for the O_2 $3d\pi_g$ Rydberg states. Bands from transitions to $4s\sigma_g$ and $3d\sigma_g$ Rydberg levels are also present. The upper panel shows transitions from $X\ ^3\Sigma_g^-$ to these levels, while the lower panel shows transitions from O_2 $a\ ^1\Delta_g$. The middle panel shows our calculated electronic state positions and their percent triplet character at $J = 0$. All of the labeled states are of g symmetry. The zero of energy is 86 803 cm^{-1}.

ized in Tables III–VIII. Additional spectra are presented elsewhere.[77] To aid in the assignments, we have classified groups of $3d\pi_g$ transitions as series 1 through series 8, and we have labeled additional features as *.

The *series 1, 2,* and *3* transitions (Figs. 3–5) arise from excitations to an electronic state with vibrational levels $v' = 0$–5 at 10.625, 10.857, 11.086, 11.309, 11.529, and 11.748 eV, respectively. (Unless otherwise specified, state energies reported in this work are based on the position of the strongest peak and are measured relative to the lowest vibrational level of the ground state.) The initial state of the series-1 transitions is $X\ ^3\Sigma_g^-$, for series 2 it is O_2 $a\ ^1\Delta_g$, and for series 3 it is $b\ ^1\Sigma_g^+$. Transitions to the vibrational levels $v' = 0$–5 of an electronic state lying 170 cm^{-1} (0.021 eV) lower in energy were observed from $a\ ^1\Delta_g$ only (See Fig. 5.) These transitions comprise *series 4*.

Series 6, also illustrated in Fig. 5, corresponds to a very weak transition from O_2 $a\ ^1\Delta_g$ to a state at 10.798 eV. No other vibrational bands were observed for that transition. However, bands for transitions from the $v'' = 0$ level of $X\ ^3\Sigma_g^-$ to vibrational levels at about 10.572, 10.800, 11.021, and 11.243 eV were observed, and comprise *series 5*. The 0–0 band of series 5 is displayed in Fig. 6. These spectra are particularly complex, suggesting that several electronic states are involved.

Several weak bands with overlapping structure are also observed to the red of series 5, in transitions from $X\ ^3\Sigma_g^-$. Those bands, classified as *series 7,* begin with transitions to states lying at the energies listed in Table V and extend out to series 5. *Series 8* accesses the same energy region, but in transitions from O_2 $a\ ^1\Delta_g$. Its bands, listed in Table VIII, closely resemble doublets. Figure 7 illustrates the 0–0 bands of series 7 and 8.

Additional transitions, attributed to $4s\sigma_g$, $3d\sigma_g$, and/or $3d\delta_g$ Rydberg levels, further complicate the series-5 and series-7 spectra. Transitions attributed to $5s\sigma_g$, $4d\sigma_g$, $4d\pi_g$, and/or $4d\delta_g$ Rydberg levels, complicate the $v' \geqslant 3$ spectra for series 1–8.

Representative bands of the Rydberg transitions were examined for relative changes in intensity within the transitions as the incident laser light was varied from linear to circular polarization. The series-4 bands examined were seen to disappear completely in circularly polarized light, as

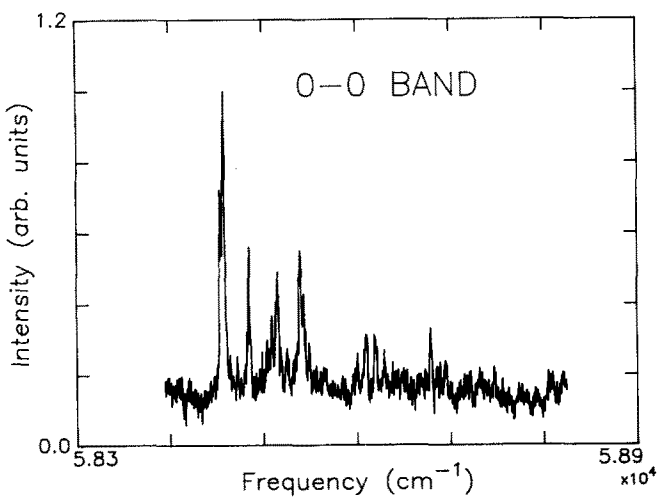

FIG. 2. The 0–0 band of the $3s\sigma_g\ ^1\Pi_g \leftarrow\leftarrow a\ ^1\Delta_g$ transition.

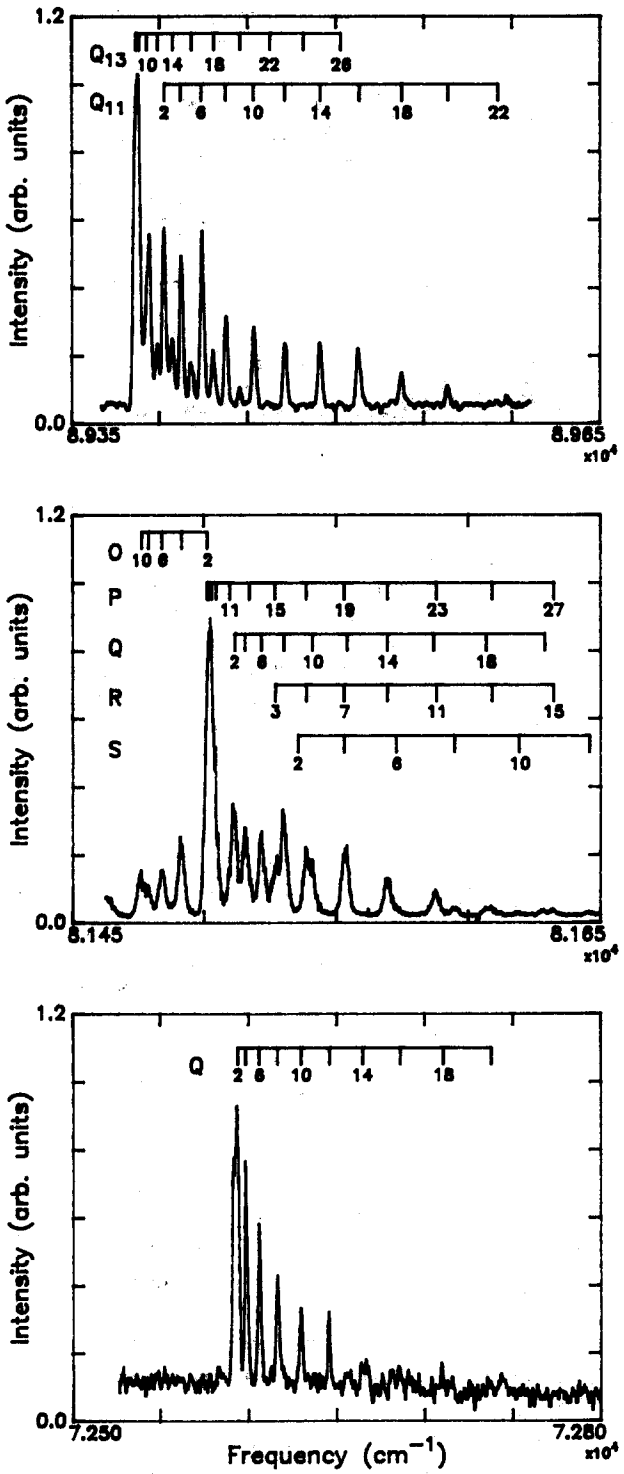

FIG. 4. (a) Spectrum and rotational assignment of the 2–0 band of the $(94\%\ ^1\Sigma_{0g}^+ \sim 6\%\ ^3\Sigma_{0g}^-) \leftarrow\leftarrow X\,^3\Sigma_g^-$ transition, series 1. For simplicity, only the Q-branch assignments are shown. The nomenclature used is as follows: Q_{13} refers to a $\Delta J = 0$ transition from the F_3 component of the lower state to the $(^1\Sigma_{0g}^+ \sim {}^3\Sigma_{0g}^-)$ upper state, while Q_{11} refers to a $\Delta J = 0$ transition from the F_1 component of the lower state to the $(^1\Sigma_{0g}^+ \sim {}^3\Sigma_{0g}^-)$ state. The numbers refer to the quantum number J of the lower state. (b) Spectrum and rotational assignment of the 2–0 band of the $(94\%\ ^1\Sigma_{0g}^+ \sim 6\%\ ^3\Sigma_{0g}^-) \leftarrow\leftarrow a\,^1\Delta_g$ transition, series 2. (c) Spectrum and rotational assignment of the 0–0 band of the $(94\%\ ^1\Sigma_{0g}^+ \sim 6\%\ ^3\Sigma_{0g}^-) \leftarrow\leftarrow b\,^1\Sigma_g^+$ transition, series 3. For simplicity, only the Q-branch assignments are shown.

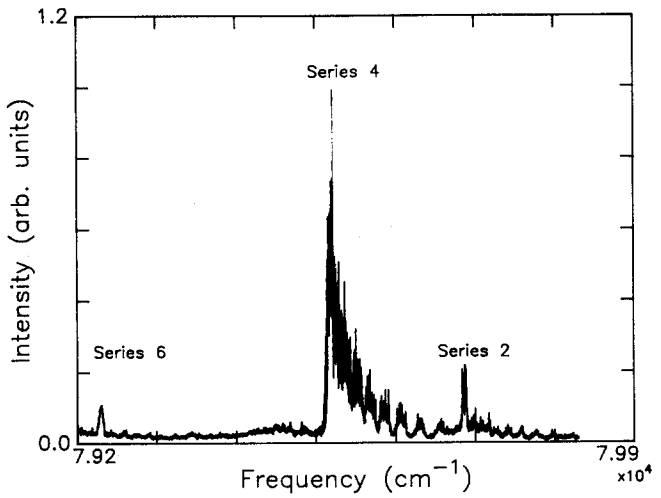

FIG. 5. 1–0 bands of series 2, 4, and 6, corresponding to the $(94\%\ ^1\Sigma_{0g}^+ \sim 6\%\ ^3\Sigma_{0g}^-) \leftarrow\leftarrow a\,^1\Delta_g$, $(97\%\ ^1\Delta_{2g} \sim 3\%\ ^3\Delta_{2g}) \leftarrow\leftarrow a\,^1\Delta_g$, and $(94\%\ ^3\Sigma_{0g}^- \sim 6\%\ ^1\Sigma_{0g}^+) \leftarrow\leftarrow a\,^1\Delta_g$ transitions, respectively.

shown in Fig. 8. Similarly, the intensities of the series-1 bands and of portions of the series-5 bands were greatly reduced in circularly polarized light. This behavior is characteristic of $\Delta\Omega = 0$ contributions to the transition's oscillator strength.[67] No change in relative branch intensities was observed for transitions of series 2, 7, and 8, although the absolute signal levels obtained with circularly polarized light were approximately 3/2 those obtained with linearly polarized light, behavior characteristic of $\Delta\Omega \neq 0$ contributions.[66] Similarly, transitions originating from O_2 $a\,^1\Delta_g$ to the

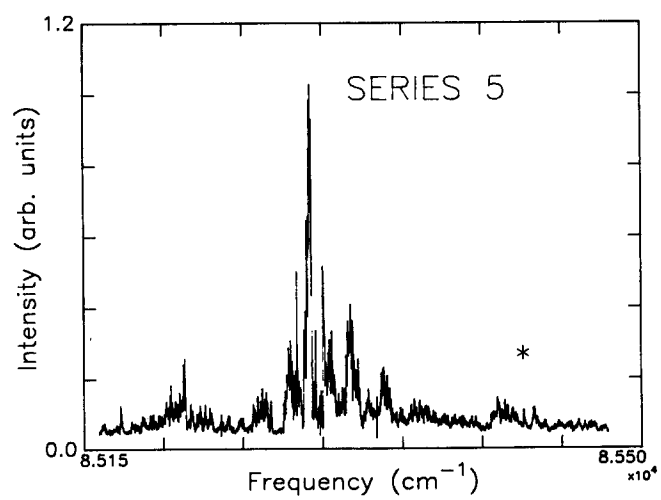

FIG. 6. 0–0 bands of series 5, the $(94\%\ ^3\Sigma_{0g}^- \sim 6\%\ ^1\Sigma_{0g}^+) \leftarrow\leftarrow X\,^3\Sigma_g^-$ and $(94\%\ ^3\Sigma_{1g}^- \sim 6\%\ ^3\Sigma_{1g}^+) \leftarrow\leftarrow X\,^3\Sigma_g^-$ transitions. The feature labeled * corresponds to either the 0–0 band of the $4s\sigma_g$ or $3d\delta_g$ $^3\Pi_g \leftarrow\leftarrow X\,^3\Sigma_g^-$ transition, or the 1–0 band of the $3d\sigma_g$ $^3\Pi_g \leftarrow\leftarrow X\,^3\Sigma_g^-$ transition. Additional structure at the low-energy side of the spectrum may arise from a transition terminating on a $4s\sigma_g$, $3d\delta_g$, or $3d\sigma_g$ level which is not responsible for feature *.

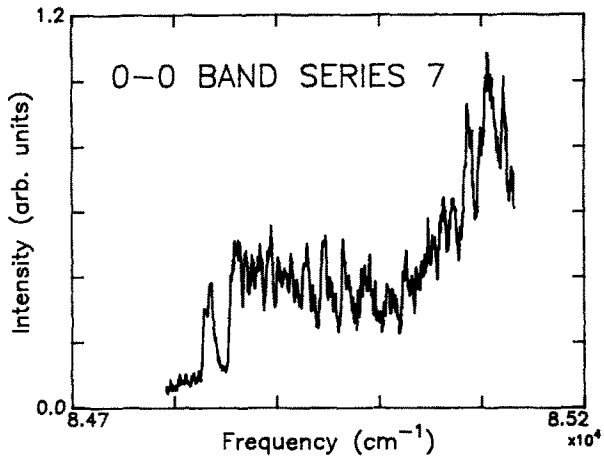

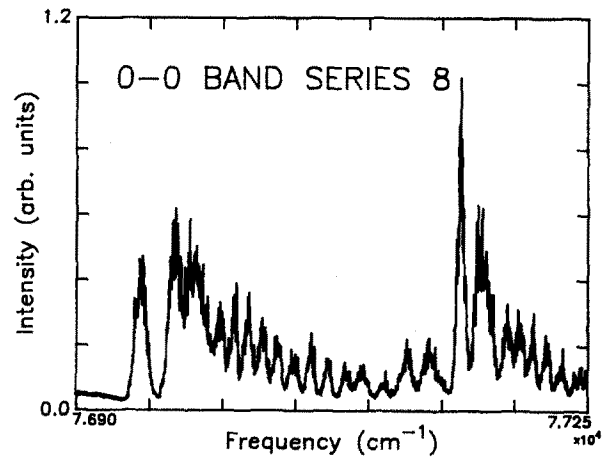

FIG. 7. (a) The 0–0 bands of series 7. Series 7 includes the $^3\Delta_{1g} \leftarrow\leftarrow X\,^3\Sigma_g^-$, $(94\%\ ^3\Sigma_{1g}^+ \sim 6\%\ ^3\Sigma_{1g}^-) \leftarrow\leftarrow X\,^3\Sigma_g^-$, $(97\%\ ^3\Delta_{2g} \sim 3\%\ ^1\Delta_{2g}) \leftarrow\leftarrow X\,^3\Sigma_g^-$, and $^3\Delta_{3g} \leftarrow\leftarrow X\,^3\Sigma_g^-$ transitions. Further spectral complication may arise from transitions to $3d\sigma_g$, $3d\delta_g$, and/or $4s\sigma_g$ Rydberg levels. (b) The 0–0 bands of series 8, including the two $(50\%\ ^3\Sigma_{0g}^+ \sim 50\%\ ^1\Sigma_{0g}^-) \leftarrow\leftarrow a\,^1\Delta_g$ transitions. Conceivably, a $(97\%\ ^3\Delta_{2g} \sim 3\%\ ^1\Delta_{2g}) \leftarrow\leftarrow a\,^1\Delta_g$ transition could also be present, but it is probably too weak to observe. Further spectral complications may arise from transitions to $3d\sigma_g$, $3d\delta_g$, and/or $4s\sigma_g$ Rydberg levels.

TABLE III. Observed $3d\pi_g$ series 1 bands in the multiphoton ionization of O_2.

Lower state	Upper v'	Wavelength[a] (nm)	Energy[b] (eV)	Energy[b] (cm^{-1})
$X\,^3\Sigma_g^-$ Series 1	0	233.4	10.625	85 697
$X\,^3\Sigma_g^-$ Series 1	1	228.4	10.856	87 564
$X\,^3\Sigma_g^-$ Series 1	2	223.7	11.083	89.394
$X\,^3\Sigma_g^-$ Series 1	3	219.3	11.308	91 205

[a] Air-to-vacuum corrected.
[b] Energies quoted correspond to ν_{i0}.

TABLE IV. Observed $3d\pi_g$ series 2 bands in the multiphoton ionization of O_2.

Lower state	Upper v'	Wavelength[a] (nm)	Energy[b] (eV)	Energy[b] (cm^{-1})
$a\,^1\Delta_g$ Series 2	0	257.0	10.625	85 695
$a\,^1\Delta_g$ Series 2	1	251.0	10.856	87 560
$a\,^1\Delta_g$ Series 2	2	245.3	11.083	89 393
$a\,^1\Delta_g$ Series 2	3	240.0	11.308	91 203
$a\,^1\Delta_g$ Series 2	4	235.0(?)	11.530(?)	92 998(?)
$a\,^1\Delta_g$ Series 2	5	230.2(?)	11.748(?)	94 760(?)

[a] Air-to-vacuum corrected; (?) indicates tentative assignments.
[b] Energies quoted correspond to ν_{i0}.

TABLE V. Observed series 3, 6, and 7 $3d\pi_g$ bands in the multiphoton ionization of O_2.

Lower state	Upper v'	Wavelength[a] (nm)	Energy[b] (eV)	Energy[b] (cm^{-1})
$b\,^1\Sigma_g^+$ Series 3	0	275.5	10.624	85 693
$a\,^1\Delta_g$ Series 6	1	252.4	10.798	87 097
$X\,^3\Sigma_g^-$ Series 7	0	235.7[c]	10.519	84 839
$X\,^3\Sigma_g^-$ Series 7	1	230.6[c]	10.751	86 715
$X\,^3\Sigma_g^-$ Series 7	3	221.2[c]	11.206	90 382

[a] Not air-to-vacuum corrected, except for series 3.
[b] Except for series 3, energies measured relative to the lowest vibrational level of the ground state. The series-3 energy corresponds to ν_{00}.
[c] Only the $^3\Delta_{1g}$ state is listed.

TABLE VI. Observed $3d\pi_g$ series 4 bands in the multiphoton ionization of O_2.

Lower state	Upper v'	Wavelength[a] (nm)	Energy[b] (eV)	Energy[b] (cm^{-1})
$a\,^1\Delta_g$ Series 4	0	257.6	10.603	85 517
$a\,^1\Delta_g$ Series 4	1	251.5	10.834	87 382
$a\,^1\Delta_g$ Series 4	2	245.8	11.063	89 231
$a\,^1\Delta_g$ Series 4	3	240.5	11.286	91 026
$a\,^1\Delta_g$ Series 4	4	235.5(?)	11.505(?)	92 796(?)
$a\,^1\Delta_g$ Series 4	5	230.7(?)	11.723(?)	94 555(?)

[a] Not air-to-vacuum corrected; positions based on band center; (?) indicates tentative assignments.
[b] Energies measured relative to the lowest vibrational level of the ground state.

TABLE VII. Observed $3d\pi_g$ series 5 bands in the multiphoton ionization of O_2.

Lower state	Upper v'	Wavelength[a] (nm)	Energy[b] (eV)	Energy[b] (cm^{-1})
$X\,^3\Sigma_g^-$ Series 5	0	234.5	10.572	85 272
$X\,^3\Sigma_g^-$ Series 5	1	229.5	10.800	87 110
$X\,^3\Sigma_g^-$ Series 5	2	224.9	11.021	88 891
$X\,^3\Sigma_g^-$ Series 5	3	220.5(?)	11.243(?)	90 686(?)

[a] Not air-to-vacuum corrected; positions based on band center; (?) indicates tentative assignment. Additional features from a $3d\sigma_g$, $3d\delta_g$, or $4s\sigma_g\ ^3\Pi_g \leftarrow\leftarrow X\,^3\Sigma_g^-$ transition are seen at 10.587, 10.817, 11.045, and 11.267 eV. (See Secs. IV D 3 and IV E.)

[b] Energies measured relative to the lowest vibrational level of the ground state.

$3s\sigma_g\ ^1\Pi_g$ Rydberg level also displayed $\Delta\Omega \neq 0$ polarization behavior. (See Sec. IV B.) We did not have the opportunity to check the behavior of series 3 and 6 with circularly polarized light, but based on our assignments (see Secs. IV D 1 and IV D 3), we expect that series 3 should also have been greatly reduced in intensity with circularly polarized light, while series 6 should have shown only the 50% increase in intensity.

IV. DISCUSSION

A. The $3s\sigma_g$ Rydberg levels: $^3\Pi_g$ and $^1\Pi_g$

Several MPI transitions from $X\,^3\Sigma_g^-$ and $a\,^1\Delta_g$ to the $3s\sigma_g\ ^{1,3}\Pi_g$ states have already been reported by other groups.[10–13] In addition to confirming those reported bands, we have obtained spectra for several new bands. (See Tables I and II.)

One of those bands previously unobserved in MPI, the $^1\Pi_g \leftarrow\leftarrow {}^1\Delta_g$ 0–0 band, is displayed in Fig. 2. We have found that the signals for the corresponding 1–0, 2–0, and 3–0 bands are well over an order of magnitude more intense than signals obtained for this band, while all bands of the analogous $^1\Pi_g \leftarrow\leftarrow {}^3\Sigma_g^-$ transition are of roughly similar intensity. This behavior is consistent with the fact that four photons are required to ionize O_2 $a\,^1\Delta_g$ at the 0–0 band wavelength, resulting in a smaller cross section for the 2 + 2 process than for the 2 + 1 processes operative in the other transitions.[12] In addition, a dissociative state of oxygen lies at the energy

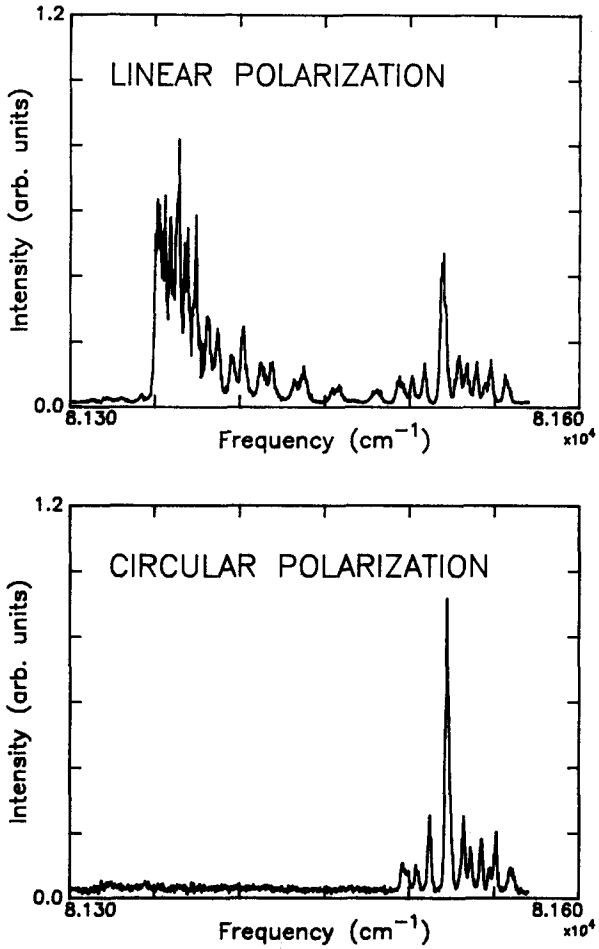

FIG. 8. The 2–0 band of the (97% $^1\Delta_{2g} \sim 3\%\ ^3\Delta_{2g}) \leftarrow\leftarrow a\,^1\Delta_g$ transition, series 4, recorded using linear and circular polarization.

TABLE VIII. Observed $3d\pi_g$ series 8 bands in the multiphoton ionization of O_2.

Lower state	Upper v'	Wavelength[a] (nm)	Energy[b] (eV)	Energy[b] (cm^{-1})
$a\,^1\Delta_g$ Series 8	0	259.9, 259.2	10.518, 10.542	84 834, 85 026
$a\,^1\Delta_g$ Series 8	1	253.7, 253.0[c]	10.751, 10.776	86 714, 86 914
$a\,^1\Delta_g$ Series 8	2	247.8, 247.2	10.980, 11.006	88 562, 88 773
$a\,^1\Delta_g$ Series 8	3	242.4, 241.8	11.205, 11.232	90 377, 90 593
$a\,^1\Delta_g$ Series 8	4	237.3, 236.6	11.429, 11.457	92 181, 92 406
$a\,^1\Delta_g$ Series 8	5	c, 231.7	c, 11.679	c, 94 197

[a] Not air-to-vacuum corrected; positions based on band center. The spectra in this region may be complicated by other states. (See Secs. IV D 4 and IV E.)

[b] Energies measured relative to the lowest vibrational level of the ground state.

[c] Weak.

sum of three $\simeq$340 nm photons,[12,51] possibly resulting in a competition between dissociation and ionization.

Comparisons of spectra in the 301–303 nm wavelength region recorded with the microwave discharge on and off show that additional well-resolved peaks appear when the microwave discharge is on, corresponding to the 4–0 band of the $^1\Pi_g \leftarrow\leftarrow {}^1\Delta_g$ transition.[77] (Based on its excitation energy, this transition might also be assigned as the 1–1 band of the $^3\Pi_g \leftarrow\leftarrow {}^3\Sigma_g^-$ transition, expected to lie at 302.5 nm, but that band should be as poorly resolved as the 1–0 band, observed at 295.4 nm.) These peaks are partially obscured by the 0–0 bands of the $^3\Pi_g \leftarrow\leftarrow {}^3\Sigma_g^-$ and $^1\Pi_g \leftarrow\leftarrow {}^3\Sigma_g^-$ transitions. Similarly, an additional feature appearing in the MPI spectrum of the $3s\sigma_g$ $^3\Pi_g \leftarrow\leftarrow {}^3\Sigma_g^-$ 1–0 band when the microwave discharge is on may be the 5–0 band of the $3s\sigma_g$ $^1\Pi_g \leftarrow\leftarrow {}^1\Delta_g$ transition at $\sim$295 nm.[77] The positions of all of the $3s\sigma_g$ $^3\Pi_g$ and $^1\Pi_g$ bands observed in this work are consistent with the recent kinetic energy release measurements of van der Zande *et al.*,[37] which located the $v = 0$–8 levels for both the $^3\Pi_g$ and $^1\Pi_g$ electronic states.

B. The 1 $^1\Pi_g$ and 2 $^1\Pi_g$ valence levels

The presence of an additional state or states complicates our $3s\sigma_g$ $^1\Pi_g \leftarrow\leftarrow {}^1\Delta_g$ spectra immensely. Johnson, Long, and Hudgens[12] noted this complexity previously, and pointed out that two-photon selection rules do little to limit the number of contenders for the guilty state or states, as transitions to Σ, Π, Δ, Φ, and Γ symmetries are all allowed from O_2 a $^1\Delta_g$. They assigned bands at 331.3 and 312.2 nm to the 1–0 and 3–0 bands, respectively, of the $3s\sigma_g$ $^1\Pi_g \leftarrow\leftarrow {}^1\Delta_g$ transition, a weak band at 324.8 nm to the 2–0 band of the $3s\sigma_g$ $^3\Pi_g \leftarrow\leftarrow {}^1\Delta_g$ transition, and structure at 311.3 nm to the 0–1 band of the $3s\sigma_g$ $^3\Pi_g \leftarrow\leftarrow {}^3\Sigma_g^-$ transition. Several other bands remained unassigned, although Johnson, Long, and Hudgens noted that portions of the group of features in the 319.5–322 nm region should correspond to the 2–0 band of the $3s\sigma_g$ $^1\Pi_g \leftarrow\leftarrow {}^1\Delta_g$ transition.

We concur with the $3s\sigma_g$ $^1\Pi_g \leftarrow\leftarrow a$ $^1\Delta_g$ assignments of Johnson, Long, and Hudgens,[12] although we disagree with the assignment of the 311.3 nm feature to a transition from vibrationally excited ground-state O_2 to $v = 0$ of the $3s\sigma_g$ $^3\Pi_g$ state. Our spectra of that feature show resolvable structure, yet the $v = 0$ level of the $^3\Pi_g$ state is known to be severely predissociated in all spin–orbit components, as are the $v = 1$ and $v = 3$ levels. Perhaps this band can be included in a series with the other unassigned bands that show resolved rotational structure at 320.7 and 330.7 nm. Possibly, the feature at 341.3 nm should also be included in this series.

The "mystery" state or states responsible for these unassigned transitions is still unknown. The calculations of Cartwright *et al.*[4] showed no gerade Rydberg states in this region, other than the $3s\sigma_g$ $^3\Pi_g$ and $^1\Pi_g$ states. The $3d\delta_g$ states, which they did not consider, are expected to lie several eV higher in energy.[17,18] Our circular polarization studies showed no evidence of $\Delta\Omega = 0$ transitions in the 320.5–322.5 and 311–313 nm regions, ruling out oscillator strength contributions from Δ states.

Recently, van der Zande *et al.*[15] carefully considered the roles of Rydberg–valence and valence–valence interactions on the 1 $^1\Pi_g$ and 2 $^1\Pi_g$ valence states and the d $^1\Pi_g$ Rydberg state. The reader is referred to their work for a further discussion of the states contributing to these transitions.

C. Spin-orbit coupling in the $3s\sigma_g$ and $3d\pi_g$ Rydberg levels

The levels arising from the $3s\sigma_g$ Rydberg configuration are more closely described by (Λ,S) coupling than by (Ω_c,ω) coupling, as supported by the fact that the splitting between the $^3\Pi_g$ and $^1\Pi_g$ electronic states (0.09 eV) (Ref. 7) is larger than the spin–orbit splitting of the $^3\Pi_g$ components (105 $cm^{-1} = 0.013$ eV).[13] Nevertheless, considerations of (Ω_c,ω) coupling clarify many observations relating to the $3s\sigma_g$ Rydberg transitions. In particular, they explain the measurements of Katsumata *et al.*[13] which showed spin–orbit splittings of F_1–$F_2 = 84$ and F_2–$F_3 = 106$ cm^{-1}. Uneven spin–orbit splittings are an indication of mixing between singlet and triplet levels. For example, an instance in which a $^3\Delta_2$ level is shifted to higher energy than both the $^3\Delta_1$ and $^3\Delta_3$ levels has been documented in CaO.[78]

Of the $\Omega = 2, 1, 1, 0^+, 0^-$ states which result from the coupling of the $3s\sigma_g$ Rydberg electron to the O_2^+ $^2\Pi_{3/2,1/2}$ core, only the $\Omega = 1$ states may couple with each other, due to the $\Delta\Omega = 0$ selection rule. Hence, two states, each of mixed $^1\Pi_{1g}$ and $^3\Pi_{1g}$ character result. One level is still primarily $^1\Pi_{1g}$ in character, with a little $^3\Pi_{1g}$ character mixed in, while the other is primarily $^3\Pi_{1g}$ in character with a little $^1\Pi_{1g}$. Unless non-Π electronic states couple to them (arising from a different molecular-orbital configuration), the remaining two spin–orbit components of $^3\Pi_g$: $^3\Pi_{0g}$ and $^3\Pi_{2g}$, will be purely triplet in character, and thus will only be observed in triplet–triplet transitions, while the spin-mixed $\Omega = 1$ states may be observed in transitions from both singlet and triplet initial states.

Spin-orbit mixing is much more important in the $3d\pi_g$ Rydberg states because of the smaller energy separations of the zero-order (Λ,S) states. In the (Λ,S) coupling limit, the states arising from the addition of a π Rydberg electron to a $^2\Pi$ ion core are $^{1,3}\Sigma_g^-$, $^{1,3}\Sigma_g^+$, and $^{1,3}\Delta_g$. In the (Ω_c,ω) limit appropriate for large spin–orbit coupling, the states are labeled as $\Omega = 1, 0^+, 0^-, 2, 1, 2, 1, 3, 0^+$, and 0^-. The Appendix provides an examination of how the spin–orbit matrix elements can be used in conjunction with the so-called Recknagel parameters to predict the energies of the $3d\pi_g$ Rydberg states. The calculation has four parameters, the three Recknagel parameters a, b, and c, and the matrix element a_π. The last of these is required to be similar to the spin–orbit splitting of the $v = 0$ O_2^+ ion, 200.33 cm^{-1}. We have used 197.3 cm^{-1} as an average for the levels $v = 0$–5. The parameters a, b, and c were adjusted to give the best fit to the data, with the result that $a = b = 95$ cm^{-1} and $c = 280$ cm^{-1}. The calculation results in eigenvalues and eigenvectors for the resulting levels, as summarized in Table IX. These energies and eigenvalues have been used in conjunction with the polarization data and spectral simulations to assign the spectra.

It is interesting to compare the values of the Recknagel parameters a, b, and c to values for similar systems. An examination of the constants for N_2, CO, CS, and SiO (Ref.

TABLE IX. Eigenvalues and eigenvectors for spin–orbit levels. (Constants: $a = b = 95.0\ cm^{-1}$; $c = 280\ cm^{-1}$; $a_\pi/2 = 98.65\ cm^{-1}$.)

Energy (cm^{-1})	Eigenvector
− 98.65	$\Psi_{f,e} = 1.00\Psi^0(^3\Delta_1)$
− 98.65	$\Psi_f = 0.707\Psi^0(^3\Sigma_0^+) - 0.707\Psi^0(^1\Sigma_0^-)$
− 24.66	$\Psi_f = +0.970\Psi^0(^3\Sigma_1^+) - 0.243\Psi^0(^3\Sigma_1^-)$ $\Psi_e = -0.970\Psi^0(^3\Sigma_1^+) + 0.243\Psi^0(^3\Sigma_1^-)$
− 16.87	$\Psi_f = +0.986\Psi^0(^3\Delta_2) - 0.169\Psi^0(^1\Delta_2)$ $\Psi_e = -0.986\Psi^0(^3\Delta_2) + 0.169\Psi^0(^1\Delta_2)$
98.65	$\Psi_f = -1.00\Psi^0(^3\Delta_3)$ $\Psi_e = +1.00\Psi^0(^3\Delta_3)$
98.65	$\Psi_f = 0.707\Psi^0(^3\Sigma_0^+) + 0.707\Psi^0(^1\Sigma_0^-)$
345.9	$\Psi_e = 0.971\Psi^0(^3\Sigma_0^-) - 0.237\Psi^0(^1\Sigma_0^+)$
394.7	$\Psi_f = -0.970\Psi^0(^3\Sigma_1^-) - 0.243\Psi^0(^3\Sigma_1^+)$ $\Psi_e = +0.970\Psi^0(^3\Sigma_1^-) + 0.243\Psi^0(^3\Sigma_1^+)$
576.9	$\Psi_{f,e} = 0.986\Psi^0(^1\Delta_2) + 0.169\Psi^0(^3\Delta_2)$
774.1	$\Psi_e = -0.971\Psi^0(^1\Sigma_0^+) - 0.237\Psi^0(^3\Sigma_0^-)$

79) shows two trends. First, these $\pi^3\pi'$ configurations all share the property that $a \approx b \ll c$. This relationship becomes a better approximation as the charge distribution in the molecule becomes more symmetric. Second, the values of all three parameters become smaller as the π and π' orbitals become progressively more localized onto separate atoms. In the case of the $\pi\pi'$ Rydberg configuration of O_2 under examination here, the localization involves one core orbital and one Rydberg orbital. Such Rydberg localization has been discussed by Ermler and Mulliken for the case of the $1\pi_u\ ^3 1\pi_g$ valence configuration ($1\pi_u$ and $1\pi_g$ are both valence orbitals) compared to the $1\pi_u\ ^3 2\pi_u$ Rydberg configuration in N_2.[80] The values of a, b, and c are approximately an order of magnitude smaller for the Rydberg configuration than for the valence configuration. It is not surprising then to find for the O_2 Rydberg configuration under study that the values of a, b, and c ($a = b = 95 cm^{-1}$, $c = 260\ cm^{-1}$) are all relatively small and that they obey the relationship $a \approx b \ll c$.

D. The $3d\pi_g$ Rydberg levels

We have assigned eight series that we have observed as transitions leading to $3d\pi_g$ Rydberg levels. (See Figs. 3–7 and Tables III–VIII.) One justification for these assignments is that the $v' = 0$ bands of series 1–8 lie close in energy to the levels calculated by Cartwright *et al.*[4] for the $^{1,3}\Sigma_g^-$, $^{1,3}\Sigma_g^+$, and $^{1,3}\Delta_g$ terms arising from the $3d\pi_g$ Rydberg configuration. Further confirmation of the Rydberg character of the observed spectra comes from closer examination of series 8. (See Figs. 3 and 7.) Each band of this series consists of two pairs of features separated by $\simeq 200\ cm^{-1}$ in energy, an amount consistent with the known splitting of 200.33 cm^{-1} between the $^2\Pi_{3/2}$ and $^2\Pi_{1/2}$ terms of the $v = 0$ O_2^+ ion.[81] However, the energy separations between the features in the 0–0 bands for series 1–8 (Tables III–VIII) do not correspond to the separations between the terms calculated by Cartwright *et al.*[4] Instead, a detailed analysis (see the Appendix) shows that these levels are better described as intermediate between (Ω_c,ω) coupling and (Λ,S) coupling rather than by the (Λ,S) coupling limit assumed by Cartwright *et al.*[4] The remainder of the discussion will refer to the results of the calculation outlined in the Appendix and summarized in Table IX. Figure 3 provides a pictorial summary and is useful in following the discussion below.

1. Series 1, 2, and 3

We propose that the Rydberg state responsible for series 1, 2, and 3 (see Fig. 4) is the upper component of a ($^1\Sigma_{0g}^+ \sim {}^3\Sigma_{0g}^-$) pair; expressed in a Hund's case (a) basis set it can be described as a mixture of 94% $^1\Sigma_{0g}^+$ and 6% $^3\Sigma_{0g}^-$. [These compositions here and in the following discussion refer only to $J = 0$. For $J > 0$, effects from the $-B(J^+S^- + J^-S^+)$ spin-uncoupling operator must be taken into account.] Consequently, we might expect to observe transitions arising from both $O_2\ a\ ^1\Delta_g$ and $X\ ^3\Sigma_g^-$ to this state, and indeed, we do. Furthermore, a transition from $O_2\ b\ ^1\Sigma_g^+$ to this state is also allowed. We attribute series 1 to the transition from $^3\Sigma_g^-$ to this state, series 2 to the corresponding transition originating from $O_2\ a\ ^1\Delta_g$, and series 3 to the transition from $b\ ^1\Sigma_g^+$. Thus, series 2 should resemble a $\Sigma \leftarrow\leftarrow \Delta$ transition, while series 1 and 3 should resemble $\Sigma \leftarrow\leftarrow \Sigma$ transitions.

The oscillator strength for the series-2 transition must come from the singlet component of the upper state, that is, the $^1\Sigma_{0g}^+$ component. A $^1\Sigma_{0g}^+ \leftarrow\leftarrow {}^1\Delta_g$ transition should have O, P, Q, R, and S branches (where O, P, Q, R, and S refer to $\Delta J = -2$, -1, 0, $+1$, and $+2$, respectively) in which antisymmetric rotational levels are absent, as required by oxygen spin statistics. Hence, odd J's will be missing in the upper state, so that the O, Q, and S branches will only have $J'' =$ even, while P and R branches will have only $J'' =$ odd. Simulations were performed for the series-2 $v' = 0$–3 bands using $B_{v'} = 1.74$, 1.721, 1.701_5, and $1.68\ cm^{-1}$, respectively. A representative result is shown for $v = 2$ in Fig. 4(b). A rotational constant of $1.417\ 81\ cm^{-1}$ was used for $O_2\ ^1\Delta_g$.[60] The signal-to-noise ratio was not adequate to evaluate quantitatively the fits for $v = 0$ and 1; we could conclude only that the rotational constants used in the simulations were consistent with the observed rotational structure. Uncertainties of ± 0.003 and ± 0.02 were estimated for B_2 and B_3, respectively.

Because the initial electronic state for the series-1 transitions is a triplet state, $X\ ^3\Sigma_g^-$, the oscillator strength for these transitions must come from the triplet component of the proposed upper state, the $^3\Sigma_{0g}^-$ component. The series-1 lines are greatly reduced in intensity when circularly polarized light is used, confirming that the oscillator strength arises from $\Sigma \leftarrow\leftarrow \Sigma$ transitions. The F_3, F_2, and F_1 triplet spin components are defined such that $J = N - 1$, $J = N$, and $J = N + 1$, respectively.[82] The state of 94% $^1\Sigma_{0g}^+$ and 6% $^3\Sigma_{0g}^-$ character is of e parity and is the higher-energy compo-

nent of the pair of spin-mixed $\Omega = 0^+$ levels. Because it is the perturbation partner of the F_1 component of the $^3\Sigma_{0g}^-$ state, its triplet character is assigned as $^3\Sigma_{0g}^- F_1$. [The F_2 component (f symmetry) and the F_3 component (e symmetry) are both $^3\Sigma_1^-$ and are nearly degenerate at low values of J (even though both are further perturbed by the $^3\Sigma_1^+$ state). The predominantly $^3\Sigma_0^- F_1$ component (e symmetry) of the ($^1\Sigma_0^+ - ^3\Sigma_0^-$) pair lies at lower energy than the F_2 and F_3 levels of the same J value.]

Much of the intensity in the series-1 transitions is carried by the Q branches, as shown by the large reduction in intensity when circularly polarized light is used. Thus, one could initially try simulations including only the Q branches. Oxygen spin statistics and e/f selection rules[83] require that Q branch transitions to this state are only allowed from F_1 or F_3 spin components of $X\,^3\Sigma_g^-$, and then, only for $J'' =$ even. We do not resolve the spin splittings within $X\,^3\Sigma_g^-$, but an additional branch,[84] especially apparent in the 2–0 band [Fig. 4(a)] arises from $\Delta J = 0$ transitions from the F_3 component of $X\,^3\Sigma_g^-$ to ($^1\Sigma_{0g}^+ - ^3\Sigma_{0g}^-$). We will refer to this additional branch as Q_{13}. The main branch, Q_{11}, arises from $\Delta J = 0$ transitions from the F_1 component of $X\,^3\Sigma_g^-$ to ($^1\Sigma_{0g}^- \sim ^3\Sigma_{0g}^-$). Including the other branches of the transition changes the appearance of the simulation only slightly, since there is a good deal of overlap between those branches and the two Q branches discussed above. Simulations for the series-1 $v' = 0$–3 bands used $B_{v'} = 1.745 \pm 0.01$, 1.721 ± 0.003, 1.7015 ± 0.002, and 1.685 ± 0.01 cm^{-1}, respectively. The $v' = 2$ simulation is shown in Fig. 4(a). A rotational constant of $B_0 = 1.438$ was used for $X\,^3\Sigma_g^-$.

A transition closely resembling the 0–0 band of series 1 was observed with the discharge on, 6559 cm^{-1} (13 118 cm^{-1} in two photons) to the red of that band. [See Fig. 4(c).] Since the splitting between the ground state of oxygen, $X\,^3\Sigma_g^-$, and the second excited state, $b\,^1\Sigma_g^+$, is 13 121 cm^{-1}, and because the spectrum of this band closely resembles that of series 1, we assign the initial state in this transition to $b\,^1\Sigma_g^+$, and the final state to this same upper component of the ($^1\Sigma_{0g}^+ \sim ^3\Sigma_{0g}^-$) pair (94% $^1\Sigma_{0g}^+$ and 6% $^3\Sigma_{0g}^-$ at $J = 0$). Downstream from the discharge, O_2 $b\,^1\Sigma_g^+$ is formed by the energy pooling process[64,85–88] suggested by Bader and Ogryzlo[85]:

$$O_2(^1\Delta_g) + O_2(^1\Delta_g) \rightarrow O_2(^1\Sigma_g^+) + O_2(^3\Sigma_g^-).$$

Because the series-3 oscillator strength comes from the $^1\Sigma_{0g}^+$ component, the transition must look like a $\Sigma \leftarrow\leftarrow \Sigma$ transition, and thus, must closely resemble series 1. As in series 1, odd levels are absent, and the Q branch is dominant in linearly polarized light. A rotational analysis of this transition [Fig. 4(c)] using a rotational constant of 1.391 27 cm^{-1} for $b\,^1\Sigma_g^+$ yielded an upper state rotational constant of $B_0 = 1.74 \pm 0.01$ cm^{-1}. We did not look for the higher-energy members of this series, but it should be possible to observe them, as well. Since we discovered this transition only during the analysis of the data, we did not have the opportunity to investigate how the laser polarization affected this band, nor whether the presence of water in the discharge quenched the signal. Also, we cannot easily compare the intensity of this band to those of series 1 and series 2, although it seems surprisingly intense when compared to the expected yields of $^1\Delta_g$ and $^1\Sigma_g^+$ from the discharge (10% and 0.001%), respectively).[89]

2. Series 4

It is clear that the upper state of the series-4 transitions must possess some $^1\Delta_g$ character, since the transitions vanish in circular polarization ($\Delta\Omega = 0$), and since they originate from O_2 $a\,^1\Delta_g$. (The transitions are observed only when the microwave discharge is on.) We have confirmed that the initial state of the transitions is not $b\,^1\Sigma_g^+$ by noting that the transitions could still be observed in the discharge when the O_2 was saturated with water vapor, an efficient quencher for $^1\Sigma_g^+$.[66] As in other $\Delta\Omega = 0$ transitions we have observed, the Q branch is dominant in linear polarization. Spin statistics do not limit the rotational lines to $J'' =$ even or odd in this type of transition. Our calculations (see the Appendix) predict that a state made up of 97% $^1\Delta_2$ and 3% $^3\Delta_2$ at $J = \Omega = 2$ will be located near this energy, perfectly consistent with our observation of a feature deriving its oscillator strength from a $^1\Delta_g \leftarrow\leftarrow {}^1\Delta_g$ transition. Simulations to the series-4 $v' = 0$–3 bands were performed using rotational constants of 1.76, 1.74, 1.72, and 1.70 cm^{-1}, respectively, but the signal-to-noise ratios were not good enough to quote rotational constants with any confidence.

3. Series 5 and series 6

Based on our calculations, we find that two $3d\pi_g$ Rydberg levels could give rise to the transitions labeled as series 5. One level can be described in Hund's case (a) basis states as 94% $^3\Sigma_{0g}^-$ and 6 % $^1\Sigma_{0g}^+$ at $J = 0$. The other level is 94% $^3\Sigma_{1g}^-$ and 6% $^3\Sigma_{1g}^+$. The complexity of the series-5 spectrum (Fig. 6) implies that both levels are observed in transitions from $X\,^3\Sigma_g^-$. Portions of series 5 were greatly reduced in intensity when circularly polarized light was used, consistent with dominant oscillator strength contributions from $\Delta\Omega = 0$ transitions. The complications of overlapping states has so far prevented us from obtaining a good simulation of series 5. The feature labeled * in Fig. 6 may arise from a transition from $X\,^3\Sigma_g^-$ to a Rydberg state of different (n,l) configuration, discussed in Sec. IV E. Because a poor signal-to-noise ratio in the region of the feature marked * resulted in inconclusive polarization results, there is also some chance that the transition could be due to a state possessing some $^3\Sigma_g^-$ character. Additional structure in the region between series 5 and 7 probably also arises from different (n,l) configurations.

Figure 5 illustrates the transition which we have assigned as series 6. We suggest that it is a transition from $^1\Delta_g$ to the ($^3\Sigma_{0g}^- \sim ^1\Sigma_{0g}^+$) predominantly $^3\Sigma_{0g}^-$ component believed to be accessed in series 5. Because of the small amount of singlet character in the upper state, the series 6 transition would be expected to be rather weak. Alternative assignments might be as a transition to a $3d\sigma_g$, $3d\delta_g$, or $4s\sigma_g$ state with some $^1\Pi_g$ character, or to a $3d\delta_g$ $^1\Phi_g$ state.

4. Series 7 and series 8

We have identified the two upper states involved in the series-8 transitions as the two components of the ($^1\Sigma_{0g}^- \sim {}^3\Sigma_{0g}^+$) pair, each a 50/50 mixture of $^1\Sigma_{0g}^-$ and $^3\Sigma_{0g}^+$. (See Fig. 7.) Once again, O_2 $a\ ^1\Delta_g$ is the initial state. The main features of this series are separated by $a_\pi \sim 200\ cm^{-1}$, as expected from our calculation.

When identical photons are used, two-photon transitions from Σ^- to Σ^+ states are identity forbidden,[90] so we did not expect to observe corresponding transitions from $X\ ^3\Sigma_g^-$ to these upper states. Nevertheless, when we looked 3941 cm^{-1} to the blue of series 8 (7883 cm^{-1} in two photons, the energy difference between the $X\ ^3\Sigma_g^-$ and $a\ ^1\Delta_g$ states of O_2), transitions did appear. We propose that these observed transitions, labeled as series 7, are not due to the two ($^1\Sigma_{0g}^- \sim {}^3\Sigma_{0g}^+$) components responsible for series 8, but to two other states degenerate with them. Our calculations show that the $^3\Delta_{1g}$ and $^3\Delta_{3g}$ states, labeled in Fig. 3, lie at the same energy as the two ($^1\Sigma_{0g}^- \sim {}^3\Sigma_{0g}^+$) components, but cannot perturb them because of the $|\Delta\Lambda| \leqslant 1$ selection rule. The situation is actually even more complicated. Another state, the lower component of the ($^1\Delta_{2g} \sim {}^3\Delta_{2g}$) pair, is calculated to be 3% $^1\Delta_{2g}$ and 97% $^3\Delta_{2g}$ at $J = \Omega = 2$ and to lie between the $^3\Delta_{1g}$ and $^3\Delta_{3g}$ states. It may be present in our spectrum. We also expect the lower component of the ($^3\Sigma_{1g}^+ \sim {}^3\Sigma_{1g}^-$) pair, consisting 94% of $^3\Sigma_{1g}^+$ and 6% of $^3\Sigma_{1g}^-$, to lie very close to the ($^3\Delta_2 \sim {}^1\Delta_2$) component. We have not seen any evidence of a transition arising from $X\ ^3\Sigma_g^-$ to this ($^3\Sigma_{1g}^+ \sim {}^3\Sigma_{1g}^-$) upper state, but this transition may be obscured by the series-7 and series-5 transitions. In summary, we assign the transitions observed in series 7 as transitions from $^3\Sigma_g^-$ to $^3\Delta_{1g}$, $^3\Delta_{3g}$, and the lower component of the ($^3\Delta_{2g} \sim {}^1\Delta_{2g}$) pair, while we assign those observed in series 8 as transitions from $^1\Delta_g$ to the two ($^1\Sigma_{0g}^- \sim {}^3\Sigma_{0g}^+$) components.

Our attempted spectral simulations of bands from series 7 and 8 have been unsuccessful. Simulations of high-resolution data from series 8 reproduce the overall spectral profile, but have fewer lines than do the data.[77] It is possible that additional rotational structure arises from transitions to the $3d\sigma_g$, $3d\delta_g$, or $4s\sigma_g$ Rydberg levels, discussed below.

E. Other Rydberg levels: $3d\sigma_g$, $3d\delta_g$, $4s\sigma_g$, $4d\sigma_g$, $4d\pi_g$, $4d\delta_g$, and $5s\sigma_g$

Calculations[4] predict that gerade levels from two other Rydberg configurations also lie in the $3d\pi_g$ energy range investigated. They are the $3d\sigma_g$ $^3\Pi_g$ and $^1\Pi_g$ states at 10.39 and 10.41 eV, and the $4s\sigma_g$ $^3\Pi_g$ and $^1\Pi_g$ states at 10.61 and 10.62 eV. Based on the vibrational spacings in the O_2^+ ion, the $v = 1$ levels of the calculated $3d\sigma_g$ $^3\Pi_g$ and $^1\Pi_g$ states could be expected to lie near 10.62 and 10.64 eV in energy.

In our spectra, we have observed features (labeled * in Figs. 3 and 6) located approximately 60 cm^{-1} higher in energy than the 0–0, 1–0, and 3–0 bands of series 5. The initial state of the transition is $X\ ^3\Sigma_g^-$, and no evidence was seen for the analogous transition from O_2 $a\ ^1\Delta_g$ to this state, suggesting that the final state is primarily triplet in character. As mentioned previously, a polarization study on the additional structure was inconclusive, so that there is some possibility that the feature is due to a $3d\pi_g$ state with some $^3\Sigma_g^-$ character. However, our calculations predict no $3d\pi_g$ states at this energy, and we consequently suggest that the additional features could correspond to a transition to one of the $^3\Pi_g$ levels predicted by Cartwright *et al.*[4] No evidence of the other triplet spin-orbit components is apparent, however.

We have also observed very weak rotational structure at about 284 nm, nestled between the 3–0 band of the $3s\sigma_g\ ^3\Pi_g \leftarrow\leftarrow {}^3\Sigma_g^-$ transition and the 2–0 band of the $3s\sigma_g\ ^1\Pi_g \leftarrow\leftarrow {}^3\Sigma_g^-$ transition. The structure can only be observed with the microwave discharge on. Energetically, the 0–0 band of a $3d\sigma_g \leftarrow b\ ^1\Sigma_g^+$ transition is plausible here. That assignment would place the upper state at an energy of about 10.36 eV, with the $v = 1$–4 vibrational levels at approximately 10.59, 10.82, 11.05, and 11.27 eV, the same energy at which we observed the "additional features" discussed in the preceding paragraph. Perhaps these features correspond to transitions from $X\ ^3\Sigma_g^-$ to a $3d\sigma_g$ state of mixed $^3\Pi_g$ and $^1\Pi_g$ character. If so, it is not clear why transitions were not observed to this state from O_2 $a\ ^1\Delta_g$. Uncertainty in the position of the band origin for the weak 284 nm transition also allows for the possibility that the transition to $3d\sigma_g$ states could contribute to series 5. Alternate assignments for this weak transition are as the 7–0 bands of the $3s\sigma_g\ ^3\Pi_g \leftarrow\leftarrow {}^1\Delta_g$ and $3s\sigma_g\ ^1\Pi_g \leftarrow\leftarrow {}^1\Delta_g$ transitions, and the 3–1 band of the $3s\sigma_g\ ^1\Pi_g \leftarrow\leftarrow X\ ^3\Sigma_g^-$ ($v = 1$) transition. Further work using an O_2 $b\ ^1\Sigma_g^+$ quencher[66] is necessary to determine the initial state of this transition.

As mentioned in the preceding section, we suspect that additional transitions to $3d\sigma_g$, $3d\delta_g$, and/or $4s\sigma_g$ Rydberg states may add to the complexity of our series 7 and 8 spectra. The spectra of series 8 appear to have too many rotational lines to be adequately simulated as only the two ($^1\Sigma_{0g}^- \sim {}^3\Sigma_{0g}^+$) $\leftarrow\leftarrow {}^1\Delta_g$ transitions discussed in Sec. IV D 4. It seems likely that series 8 may also be comprised of $3d\sigma_g\ ^1\Pi_g \leftarrow\leftarrow {}^1\Delta_g$, $3d\delta_g\ ^1\Pi_g \leftarrow\leftarrow {}^1\Delta_g$, and/or $4s\sigma_g\ ^1\Pi_g \leftarrow\leftarrow {}^1\Delta_g$ transitions, as well. Moreover, transitions from O_2 $a\ ^1\Delta_g$ to the $3d\delta_g\ ^1\Phi_g$ Rydberg state[18] cannot be ruled out, although the analogous transition from $X\ ^3\Sigma_g^-$ is symmetry forbidden. Similarly, the surfeit of rotational structure in the wavelength region between series 5 and 7 suggests that an extra $^3\Pi_g \leftarrow\leftarrow {}^3\Sigma_g^-$ transition may be hidden there, as well.

Further spectral complications arise for $v' \geqslant 3$ $3d\pi_g$ bands as transitions to $4d\sigma_g$, $4d\pi_g$, $4d\delta_g$, and $5s\sigma_g$ Rydberg states become energetically accessible.[4] Additional peaks arising from transitions to these higher-lying states are particularly striking in the 3–0 bands of series 5, 7, and 8.[77]

Table X presents a summary of our assignments as well as those for several other electronic states of O_2.

F. Comparisons with other studies

It has been suggested that several unassigned infrared emission lines observed in an O_2 discharge[35] could arise from transitions between the $3d\pi_g$ and $3p\sigma_u$ or $4p\sigma_u$ Rydberg levels. Our measurements provide some support for that suggestion by demonstrating that transitions to the $3d\pi_g$ Rydberg levels can be observed and that the levels lie very close to their calculated energies.[4]

TABLE X. Electronic states observed in this work and other nearby states.

State	Energy (cm^{-1})	Energy (eV)
$4d\sigma_g\ ^1\Pi_g$	90 180[a]	11.18[a]
$4d\sigma_g\ ^3\Pi_g$	90 090[a]	11.17[a]
$g\ ^1\Pi_u$	86 841[b]	10.767[b]
$F\ ^3\Pi_u$	86 085[b]	10.673[b]
	85 993[b]	10.662[b]
	85 902[b]	10.650[b]
$3d\pi_g$ 94% $^1\Sigma_{0g}^+$, 6% $^3\Sigma_{0g}^-$	85 695[c]	10.625[c]
$4s\sigma_g\ ^1\Pi_g$	85 660[a]	10.62[a]
$4s\sigma_g\ ^3\Pi_g$	85 580[a]	10.61[a]
$3d\pi_g$ 97% $^1\Delta_{2g}$, 3% $^3\Delta_{2g}$	85 517[d]	10.603[d]
unassigned[e]	85 394[d,e]	10.587[d,e]
$3d\pi_g$ 94% $^3\Sigma_{1g}^-$, 6% $^3\Sigma_{1g}^+$	85 260–85 320[d,f]	10.571–10.578[d,f]
$3d\pi_g$ 94% $^3\Sigma_{0g}^-$, 6% $^1\Sigma_{0g}^+$		
$3d\pi_g$ 50% $^3\Sigma_{0g}^+$, 50% Σ_{0g}^-	85 026[d,f]	10.542[d,f]
$3d\pi_g\ ^3\Delta_{3g}$		
$3d\pi_g$ 97% $^3\Delta_{2g}$, 3% $^1\Delta_{2g}$	84 857–85 200[d,f]	10.521–10.563[d,f]
$3d\pi_g$ 94% $^3\Sigma_{1g}^+$, 6% $^3\Sigma_{1g}^-$		
$3d\pi_g\ ^3\Delta_{1g}$		
$3d\pi_g$ 50% $^3\Sigma_{0g}^+$, 50% $^1\Sigma_{0g}^-$	84 834[d,f]	10.518[d,f]
$3d\sigma_g\ ^1\Pi_g$	83 960[a]	10.41[a]
$3d\sigma_g\ ^3\Pi_g$	83 800[a]	10.39[a]
$e\ ^1\Delta_{2u}$	75 382[b]	9.346[b]
$e'\ ^3\Delta_{2u}$	75 154[b]	9.318[b]
$d\ 3s\sigma_g\ ^1\Pi_g$	66 405[d,f]	8.233[d,f]
$C\ 3s\sigma_g\ ^3\Pi_g$	65 678[d]	8.143[d]
$B\ ^3\Sigma_u^-$	49 358.2[b]	6.1195[b]
$b\ ^1\Sigma_g^+$	13 120.9[b]	1.6267[b]
$a\ ^1\Delta_g$	7882.8[g]	0.9773[g]
$X\ ^3\Sigma_g^-$	0.0	0.0

[a] Reference 4.
[b] Reference 47.
[c] Average of ν_{00} values obtained from series 1, 2, and 3.
[d] Positions based on band center.
[e] See Sec. IV E.
[f] Spectrum in this region may be complicated by other electronic states.
[g] Reference 60.

Recently, Park *et al.*[17,18] reported the observation of numerous 3*d*, 4*s*, 4*d*, and 5*s* Rydberg transitions by multiphoton ionization of ground-state oxygen. Since there is considerable overlap between the wavelength regions studied by the Park *et al.* group at Yale and those studied by us, direct comparisons between the two studies are of interest.

In Ref. 18, Park *et al.* have labeled 4*s*–3*d* peaks as *A* through *L* in their spectra. For the $v' = 0$ level, features corresponding to *A*, *D*, *E*, *G*, *I*, *K*, and *L* occur at energies of 10.558, 10.562, 10.563, 10.570, 10.574, 10.587, and 10.625 eV, respectively. Also, an unlabeled feature is apparent in their Fig. 1 at 10.548 eV. It is straightforward to compare their beam measurements with our cell measurements and calculations.

The position of the unlabeled feature at 10.548 eV in the Yale spectrum makes an assignment as $^3\Delta_{3g} \leftarrow\leftarrow {}^3\Sigma_g^-$ likely. This transition is one of several which we have suggested gives rise to our series 7. Park *et al.* did not observe the weaker, longer-wavelength transitions to $^3\Delta_1$, and to the lower components of ($^3\Sigma_{1g}^+ \sim {}^3\Sigma_{1g}^-$) and ($^3\Delta_{2g} \sim {}^1\Delta_{2g}$), some of which appear in our spectra. [See Fig. 7(a)]. Features *G* and *I* in their spectra are part of the region which we have classified as series 5 in our own work. Our calculations indicate that in this region, states of (94% $^3\Sigma_{0g}^-$, 6% $^1\Sigma_{0g}^+$) and (94% $^3\Sigma_{1g}^-$, 6% $^3\Sigma_{1g}^+$) at $J = \Omega = 1$ should be split by a little less than 50 cm^{-1}. In the Yale spectra, features *G* and *I* are separated by about 40 cm^{-1}. A possible assignment, then, is with feature *G* as a transition from $^3\Sigma_g^-$ to the lower component of ($^3\Sigma_{0g}^- \sim {}^1\Sigma_{0g}^+$) and with feature *I* as a one from $^3\Sigma_g^-$ to the upper component of ($^3\Sigma_{1g}^- \sim {}^3\Sigma_{1g}^+$). Such an assignment would also be consistent with our series-6 results which located a state with some singlet character at 10.800 eV. Furthermore, our polarization results indicate that at least one feature in this region acquires oscillator strength from a $\Delta\Omega = 0$ transition starting from $^3\Sigma_g^-$. Based on the Park *et al.* photoelectron results showing a $v^+ = 1$ peak with approximately 1/3 of the intensity of the $v^+ = 0$ peak (where v^+ is the vibrational level of the ion), and on the similar behavior of higher vibrational levels, however, Park *et al.* have tentatively assigned one contribution to feature *G* as a transition from $X\ ^3\Sigma_g^-$ to a $3d\sigma_g\ ^3\Pi_g$ or $^1\Pi_g$ state.

The feature labeled *K* in the Yale spectrum corresponds to that labeled * in our Figs. 3 and 6. In Sec. IV E we have suggested that the feature could arise from $3d\sigma_g$, $3d\delta_g$, or $4s\sigma_g\ ^3\Pi_g \leftarrow\leftarrow {}^3\Sigma_g^-$ transitions, although we could not completely rule out the possibility of a $^3\Sigma_g^- \leftarrow\leftarrow {}^3\Sigma_g^-$ transition. The features labeled *A*, *D*, and *E* correspond to the congested region between series 5 and 7 in our cell spectra, where we have suggested that $3d\sigma_g$, $3d\delta_g$, and/or $4s\sigma_g$ states possessing some $^3\Pi_g$ character could contribute.

The Yale group has suggested that bands at 10.625, 10.856, 11.083, and 11.306 eV (their feature *L*, our series 1) correspond to transitions from $X\ ^3\Sigma_g^-$ to the $3d\delta\ ^1\Pi_g$ state or to the F_2 component of the $3d\delta\ ^3\Pi_g$ state. They did not see evidence for the other F_1 and F_3 components of a $^3\Pi_g$ state. Their F_2 simulations yielded $v' = 1$ and $v' = 3$ rotational constants fo 1.72 ± 0.01 and 1.68 ± 0.01 cm^{-1}, respectively. This assignment is somewhat surprising since the $3d\delta F\ ^2\Delta$ state in NO at 61 800 cm^{-1} lies at *lower* energy than the $3d\pi\ H'\ ^2\Pi$ state at 62 485 cm^{-1}. It seems likely by comparison that the $3d\delta$ states in O_2 will be below the $3d\pi$ states since the δ_g orbital is slightly bonding, whereas the π_g orbital is slightly antibonding. It also seems likely that the δ_g states will be within about 1000 cm^{-1} of the π_g states; in NO, the splitting between the π and δ states decreases from 685 cm^{-1} to 392 cm^{-1} as *n* increases from 3 to 4.

On the basis of these arguments and our own calculations, we have assigned the state giving rise to feature *L* as a state of mixed $^1\Sigma_{0g}^+$ and $^3\Sigma_{0g}^-$ character. Its polarization behavior indicates oscillator strength contributions from $\Delta\Omega = 0$ transitions, and our calculations place the mixed state at this energy. Our rotational constants for the 1–0 and 3–0 bands agree with those obtained by Park *et al.* in their $\Pi \leftarrow\leftarrow \Sigma$ simulations. We were also able to obtain constants from the 0–0 and 2–0 bands. Our spectra and simulations of the transitions from $O_2\ a\ ^1\Delta_g$ and $b\ \Sigma_g^+$ to this state (series 2 and 3) were consistent with an assignment as a state of

mixed $^1\Sigma_{0g}^+$ and $^3\Sigma_{0g}^-$ character. We place the $3d\delta$ states lower in energy; they possibly contribute to the feature marked * in our spectrum and/or to the unresolved features in series 5–8.

Finally, we proposed that the very weak feature at 85 520 cm^{-1} (see Fig. 1 of Ref. 17) and the very weak peaks at 87 390 cm^{-1} in the Park *et al.* spectra are the 0–0 and 1–0 bands, respectively, of the transition from $^3\Sigma_g^-$ to the upper component of ($^1\Delta_{2g} \sim {}^3\Delta_{2g}$), the transition analogous to our series 4, but arising from a different initial state.

V. CONCLUSIONS

Multiphoton ionization spectroscopy of O_2 $X\,^3\Sigma_g^-$, $a\,^1\Delta_g$, and $b\,^1\Sigma_g^+$ has provided spectra of numerous bands arising from transitions to Rydberg states of the $3s\sigma_g$, $3d\sigma_g$, $3d\pi_g$, $3d\delta_g$, and $4s\sigma_g$ configurations. These bands probe upper state vibrational levels from $v' = 0$–5. Our $3s\sigma_g$ spectra are consistent with previous measurements, and we report additional MPI bands, notably the 0–0 band of the $^1\Pi_g \leftarrow\leftarrow {}^1\Delta_g$ transition. Our $3d\pi_g$ measurements agree with the calculations of Cartwright *et al.*[4] to within 0.01–0.06 eV, but our analysis has taken into account the mixing induced by spin–orbit coupling. We have also seen evidence of transitions to higher-lying $4d$ and $5s$ Rydberg states. Our polarization measurements have assisted in the assignments by identifying spectral features deriving oscillator strength from $\Delta\Omega = 0$ transitions. There is some overlap between our studies of $^3\Sigma_g^-$ transitions and the work recently reported by Park *et al.*[17,18] The spectra are in reasonable agreement, but our assignments differ from theirs. The new assignments, summarized in Table X, will be of importance in using the $3d\pi_g$ Rydberg states as intermediates both in the MPI detection of O_2 and in the preparation of state-selected O_2^+ ions.

ACKNOWLEDGMENTS

This work was supported by the Air Force Office of Scientific Research under Grant No. AFOSR-87-0017. We are grateful to Dr. G. E. Hall for assistance on some of the experimental work and to Dr. A. Sur for comments on the manuscript.

APPENDIX: SPIN–ORBIT COUPLING OF THE ($3d\pi_g$) RYDBERG LEVELS

We consider as a starting point the terms arising from a $\cdots(\pi_g 2p)(3d\pi_g)$ Rydberg configuration: $^{1,3}\Sigma_g^-$, $^{1,3}\Sigma_g^+$, and $^{1,3}\Delta_g$. The splitting between these terms has been considered Recknagel[91] and is described by parameters a, b, and c, which for any particular system are constants related to direct and exchange Coulomb integrals. For a $\pi\pi'$ configuration one obtains the following:

$$\begin{aligned}
&^3\Sigma^+, \quad E + a - b,\\
&^3\Delta, \quad E,\\
&^3\Sigma^-, \quad E + 2c - a - b,\\
&^1\Sigma^-, \quad E - a + b,\\
&^1\Delta, \quad E + 2c,\\
&^1\Sigma^+, \quad E + 2c + a + b.
\end{aligned} \tag{A1}$$

We now consider the spin–orbit interaction between the $^{1,3}\Sigma_g^-$, $^{1,3}\Sigma_g^+$, and $^{1,3}\Delta_g$ terms arising from the $\cdots(\pi_g 2p)(3d\pi_g)$ Rydberg configuration. A general spin–orbit Hamiltonian can be written as[92,93]

$$H^{SO} = \sum \hat{a}_i l_i \cdot S_i, \tag{A2}$$

where $\hat{a}_i$ is an operator which acts only on the radial part of the wave function and is dependent on the effective nuclear charge. The dot product in Eq. (A2) can be expanded to give

$$l_i \cdot S_i = l_{iz} S_{iz} + \tfrac{1}{2}(l_i^+ S_i^- + l_i^- S_i^+). \tag{A3}$$

The selection rules for this operator are given by[94]

$$\begin{aligned}
&\Delta J = 0, \quad \Delta\Omega = 0,\\
&g \leftarrow/\rightarrow u, \quad e \leftarrow/\rightarrow f, \quad \Sigma^+ \leftrightarrow \Sigma^-,\\
&\Delta S = 0, \pm 1,\\
&\Delta\Lambda = \Delta\Sigma = 0 \quad \text{or} \quad \Delta\Lambda = -\Delta\Sigma = \pm 1.
\end{aligned} \tag{A4}$$

TABLE XI. Wave functions arising from a $\pi\pi'$ configuration.

Term	$\lvert\Lambda,\Sigma,\Omega,S\rangle$	Wave function [a]
$^1\Delta$	$\lvert \pm 2,0, \pm 2,0\rangle$	$(1/2)(\pi^{\pm}\pi'^{\pm} + \pi'^{\pm}\pi^{\pm})(\alpha\beta - \beta\alpha)$
$^3\Delta$	$\lvert 2,1,3,1\rangle$	$2^{-1/2}(\pi^+\pi'^+ - \pi'^+\pi^+)\alpha\alpha$
	$\lvert -2,1,-1,1\rangle$	$2^{-1/2}(\pi^-\pi'^- - \pi'^-\pi^-)\alpha\alpha$
	$\lvert \pm 2,0, \pm 2,1\rangle$	$(1/2)(\pi^{\pm}\pi'^{\pm} - \pi'^{\pm}\pi^{\pm})(\alpha\beta + \beta\alpha)$
	$\lvert 2,-1,1,1\rangle$	$2^{-1/2}(\pi^+\pi'^+ - \pi'^+\pi^+)\beta\beta$
	$\lvert -2,-1,-3,1\rangle$	$2^{-1/2}(\pi^-\pi'^- - \pi'^-\pi^-)\beta\beta$
$^1\Sigma^{\pm}$	$\lvert 0,0,0,0\rangle$	$8^{-1/2}[(\pi^+\pi'^- \pm \pi'^+\pi^-) \pm (\pi^-\pi'^+ \pm \pi'^-\pi^+)](\alpha\beta - \beta\alpha)$
$^3\Sigma^{\pm}$	$\lvert 0,1,1,1\rangle$	$(1/2)[(\pi^+\pi'^- \mp \pi'^+\pi^-) \pm (\pi^-\pi'^+ \mp \pi'^-\pi^+)]\alpha\alpha$
	$\lvert 0,0,0,1\rangle$	$8^{-1/2}[(\pi^+\pi'^- \mp \pi'^+\pi^-) \pm (\pi^-\pi'^+ \mp \pi'^-\pi^+)](\alpha\beta + \beta\alpha)$
	$\lvert 0,-1,-1,1\rangle$	$(1/2)[(\pi^+\pi'^- \mp \pi'^+\pi^-) \pm (\pi^-\pi'^+ \mp \pi'^-\pi^+)]\beta\beta$

[a] The notation used here is a shorthand in which the first term in each product of spatial or spin factors is occupied by electron number 1 and the second term by electron number 2.

For a $\pi\pi'$ configuration, the wave functions for the (Λ,Σ)-coupled $^{1,3}\Sigma_g^-$, $^{1,3}\Sigma_g^+$, and $^{1,3}\Delta_g$ terms are given in Table XI. Application of the spin–orbit operator of Eq. (A3) to these wave functions gives the following results:

$$\begin{aligned}
&\langle {}^3\Delta_3|H^{\rm SO}|{}^3\Delta_3\rangle = \tfrac{1}{2}(a_\pi + a'_\pi) \simeq a_\pi/2,\\
&\langle {}^3\Delta_1|H^{\rm SO}|{}^3\Delta_1\rangle = -\tfrac{1}{2}(a_\pi + a'_\pi) \simeq -a_\pi/2,\\
&\langle {}^3\Delta_2|H^{\rm SO}|{}^1\Delta_2\rangle = \tfrac{1}{2}(a_\pi - a'_\pi) \simeq a_\pi/2,\\
&\langle {}^3\Sigma_1^+|H^{\rm SO}|{}^3\Sigma_1^-\rangle = \tfrac{1}{2}(a_\pi - a'_\pi) \simeq a_\pi/2,\\
&\langle {}^3\Sigma_0^+|H^{\rm SO}|{}^1\Sigma_0^-\rangle = \tfrac{1}{2}(a_\pi + a'_\pi) \simeq a_\pi/2,\\
&\langle {}^3\Sigma_0^-|H^{\rm SO}|{}^1\Sigma_0^+\rangle = \tfrac{1}{2}(a_\pi + a'_\pi) \simeq a_\pi/2. \qquad \text{(A5)}
\end{aligned}$$

In these equations, $a_\pi \equiv \langle\pi|\hat{a}|\pi\rangle$ is a one-electron integral over the $(\pi_g 2p)$ valence orbital, while $a'_\pi \equiv \langle\pi'|\hat{a}|\pi'\rangle$ is a one-electron integral over the $(3d\pi_g)$ Rydberg orbital. Because the operator $\hat{a}$ varies as $1/r^3$, a'_π will be negligible compared to a_π; this approximation yeilds the values given on the extreme right-hand side of Eq. (A5). Equations (A1) and (A5) provide a means for determination of the energies of the resulting spin–orbit mixed states relative to the $^3\Delta_2$ level. In principle, there are 16 states in all: the eight states of e symmetry include the $^1\Sigma_0^+$, the $^3\Sigma_0^-$, and the positive components of each of the $^3\Delta_{3,2,1}$, $^1\Delta_2$, $^3\Sigma_1^+$, and $^3\Sigma_1^-$, while the eight states of f symmetry include the $^1\Sigma_0^-$, the $^3\Sigma_0^+$, and the negative components of each of the $^3\Delta_{3,2,1}$, $^1\Delta_2$, $^3\Sigma_1^+$, and $^3\Sigma_1^-$. Diagonalization of the 16×16 matrix yields the desired energies.

A great deal of simplification can be obtained in the diagonalization, however, from block factorization of the 16×16 matrix. In particular, because of the selection rule $e\leftarrow/\rightarrow f$ in Eq. (A4), the 16×16 matrix contains two 8×8 blocks along its diagonal. Furthermore, because there are no elements between Σ and Δ states [see Eqs. (A4)–(A5)], each 8×8 block will contain two 4×4 blocks along its diagonal. Finally, because there are no elements between states of different Ω, each 4×4 block factors into two 2×2 blocks, and one of the 2×2 blocks factors into two 1×1 blocks. Several blocks are identical to one another. The unique blocks and the number of occurrences of each are given in Table XII.

Diagonalization of the 16×16 matrix of spin–orbit splittings relative to the $^3\Delta$ term was performed for several values of the constants a, b, c, while $a_\pi/2$ was held fixed at 98.65 cm^{-1}, the spin–orbit splitting in the O_2^+ $X\,^2\Pi$ ion. In addition to providing the eigenvalues, the diagonalization also provided eigenvectors, thereby specifying the parentage of each of the resultant levels. The results for the empirically best set of parameters are given in Table IX. It should be noted that the J-dependent l- and S-uncoupling matrix elements have been neglected in this simple picture, which is meant primarily as a guide for locating the $J=0$ levels of the spin–orbit perturbed states. Spectral simulations, which by necessity need to include $J\neq0$ levels, will need to take into account these additional perturbation mechanisms. At $J\neq0$, the transition intensities will exhibit a complex and diagnostically useful J- and e/f-dependent pattern of constructive and destructive interference effects.

TABLE XII. The unique blocks of the 16×16 matrix of eigenvalues.

e	$^1\Sigma_0^+$	$^3\Sigma_0^-$
$^1\Sigma_0^+$	$2c+a+b$	$a_\pi/2$
$^3\Sigma_0^-$	$a_\pi/2$	$2c-a-b$

e,f	$^3\Sigma_1^-$	$^3\Sigma_1^+$
$^3\Sigma_1^-$	$2c-a-b$	$a_\pi/2$
$^3\Sigma_1^+$	$a_\pi/2$	$a-b$

f	$^3\Sigma_0^+$	$^1\Sigma_0^-$
$^3\Sigma_0^+$	$a-b$	$a_\pi/2$
$^1\Sigma_0^-$	$a_\pi/2$	$b-a$

e,f	$^1\Delta_2$	$^3\Delta_2$
$^1\Delta_2$	$2c$	$a_\pi/2$
$^3\Delta_2$	$a_\pi/2$	0

e,f	$^3\Delta_1$
$^3\Delta_1$	$-a_\pi/2$

e,f	$^3\Delta_3$
$^3\Delta_3$	$a_\pi/2$

[1] L. Sanche and G. J. Schulz, Phys. Rev. Lett. **26**, 943 (1971).
[2] L. Sanche and G. J. Schulz, Phys. Rev. A **6**, 69 (1972).
[3] G. J. Schulz, Rev. Mod. Phys. **45**, 378 (1983).
[4] D. C. Cartwright, W. J. Hunt, W. Williams, S. Trajmar, and W. A. Goddard III, Phys. Rev. A **8**, 2436 (1973).
[5] R. H. Huebner, R. J. Celotta, S. R. Mielczarek, and C. E. Kuyatt, J. Chem. Phys. **63**, 241 (1975).
[6] S. Trajmar, D. C. Cartwright, and R. I. Hall, J. Chem. Phys. **65**, 5275 (1976).
[7] T. A. York and J. Comer, J. Phys. B **16**, 3627 (1983).
[8] D. Spence, J. Chem. Phys. **74**, 3898 (1981).
[9] G. E. Hall, W. Marinelli, S. Arepalli, A. T. Young, P. L. Houston, and J. R. Wiesenfeld, J. Photochem. **25**, 551 (1984).
[10] A. Sur, C. V. Ramana, W. A. Chupka, and S. D. Colson, J. Chem. Phys. **84**, 69 (1986).
[11] A. Sur, C. V. Ramana, and S. D. Colson, J. Chem. Phys. **83**, 904 (1985).
[12] R. D. Johnson III, G. R. Long, and J. W. Hudgens, J. Chem. Phys. **87**, 1977 (1987); **89**, 3930 (1988).
[13] S. Katsumata, K. Sato, Y. Achiba, and K. Kimura, J. Electron Spectrosc. Relat. Phenom. **41**, 325 (1986).
[14] P. J. Miller, L. Li, W. A. Chupka, and S. D. Colson, J. Chem. Phys. **89**, 3921 (1988).
[15] W. J. van der Zande, W. Koot, J. Los, and J. R. Peterson, J. Chem. Phys. **89**, 6758 (1988).
[16] T. Betts and V. McKoy, J. Chem. Phys. **54**, 113 (1970).
[17] H. Park, P. J. Miller, W. A. Chupka, and S. D. Colson, J. Chem. Phys. **89**, 3919 (1988).
[18] H. Park, P. J. Miller, W. A. Chupka, and S. D. Colson, J. Chem. Phys. **89**, 6676 (1988).
[19] G. J. Schulz and J. T. Dowell, Phys. Rev. **128**, 174 (1962).
[20] E. N. Lassettre, A. Skerbele, M. A. Dillon, and K. J. Ross, J. Chem. Phys. **48**, 5066 (1968).
[21] J. Geiger and B. Schröder, J. Chem. Phys. **49**, 740 (1968).
[22] M. Bixon, B. Raz, and J. Jortner, Mol. Phys. **17**, 593 (1969).
[23] R. Goldstein and F. N. Mastrup, J. Opt. Soc. Am. **56**, 765 (1966), and references therein.
[24] G. Herzberg, *Atomic Spectra and Atomic Structure* (Dover, New York, 1944), pp. 154–158.
[25] G. Herzberg, *Molecular Spectra and Molecular Structure: I. Spectra of Diatomic Molecules* (Van Nostrand, Princeton, NJ, 1950), pp. 275–280.
[26] J. P. Doering and R. McDiarmid, J. Chem. Phys. **76**, 1838 (1982).
[27] E. N. Lassettre, A. Skerbele, and M. A. Dillon, J. Chem. Phys. **50**, 1829 (1969).
[28] J. P. Doering and R. McDiarmid, J. Chem. Phys. **73**, 3617 (1980).
[29] W. A. Goddard III, D. L. Huestis, D. C. Cartwright, and S. Trajmar, Chem. Phys. Lett. **11**, 329 (1971).
[30] S. Trajmar, W. Williams, and A. Kupperman, J. Chem. Phys. **56**, 3759 (1972).
[31] D. C. Cartwright, S. Trajmar, W. Williams, and D. L. Huestis, Phys. Rev. Lett. **27**, 704 (1971).
[32] S. Trajmar, D. C. Cartwright, and W. Williams, Phys. Rev. A **4**, 1482 (1971).
[33] J. P. Doering, J. Chem. Phys. **51**, 2866 (1969).
[34] W. K. Bischel and L. E. Jusinski, Chem. Phys. Lett. **120**, 337 (1985).
[35] W. Barowy, H. Sakai, and E. S. Chang, Opt. Lett. **11**, 703 (1986).

[36]J. P. Peterson and Y. K. Bae, Phys. Rev. A **30**, 2807 (1984).
[37]W. J. van der Zande, W. Koot, J. R. Peterson, and J. Los, Chem. Phys. Lett. **140**, 175 (1987).
[38]D. C. Cartwright, N. A. Fiamengo, W. Williams, and S. Trajmar, J. Phys. B **9**, L419 (1976).
[39]H. F. Schaefer III and F. E. Harris, J. Chem. Phys. **48**, 4946 (1968).
[40]J. Leclercq, Ann. Astrophys. **30**, 93 (1967).
[41]R. J. Buenker and S. D. Peyerimhoff, Chem. Phys. **8**, 324 (1975).
[42]R. J. Buenker, S. D. Peyerimhoff, and J. Peric, Chem. Phys. Lett. **42**, 383 (1976).
[43]R. J. Buenker and S. D. Peyerimhoff, Chem. Phys. Lett. **34**, 225 (1975).
[44]R. P. Saxon and B. Liu, J. Chem. Phys. **73**, 870 (1980).
[45]R. P. Saxon and B. Liu, J. Chem. Phys. **73**, 876 (1980).
[46]R. P. Saxon and B. Liu, J. Chem. Phys. **67**, 5432 (1977).
[47]K. P. Huber and G. Herzberg, *Molecular Spectra and Molecular Structure: IV. Constants of Diatomic Molecules* (Van Nostrand Reinhold, New York, 1979), pp. 490–505.
[48]S. Chung, C. C. Lin, and E. T. P. Lee, J. Phys. B **21**, 1155 (1988).
[49]R. P. Wayne, J. Photochem. **25**, 345 (1984).
[50]E. J. Llewellyn and I. C. McDade, J. Photochem. **25**, 379 (1984).
[51]P. H. Krupenie, J. Phys. Chem. Ref. Data **1**, 423 (1972).
[52]D. Kearns, Chem. Rev. **71**, 395 (1971).
[53]*Singlet Oxygen*, edited by B. Rånby and J. F. Rabek (Wiley, New York, 1978).
[54]R. F. Heidner III, J. Photochem. **25**, 449 (1984).
[55]P. D. Whitefield, J. Photochem. **25**, 465 (1984).
[56]M. V. Zagidullin, V. I. Igoshin, and N. L. Kupriyanov, Sov. J. Quant. Electron. **17**, 320 (1987).
[57]R. F. Heidner III, C. E. Gardner, G. I. Segal, and T. M. El-Sayed, J. Phys. Chem. **87**, 2348 (1983).
[58]R. M. Badger, A. C. Wright, and R. F. Whitlock, J. Chem. Phys. **43**, 4345 (1965).
[59]R. J. Collins, D. Husain, and R. J. Donovan, J. Chem. Soc. Faraday Trans. 2 **69**, 145 (1973); S. Ogawa and M. Ogawa, Can. J. Phys. **53**, 1845 (1975).
[60]J. J. Valentini, Chem. Phys. Lett. **96**, 395 (1983); J.-C. Nieh and J. J. Valentini, J. Phys. Chem. **91**, 1370 (1987).
[61]J. H. Moore, C. C. Davis, and M. A. Coplan, *Building Scientific Apparatus* (Addison–Wesley, London, 1983), p. 191; F. C. Fehsenfield, K. M. Evenson, and H. P. Broida, Rev. Sci. Instrum. **36**, 294 (1965).
[62]L. Elias, E. A. Ogryzlo, and H. I. Schiff, Can. J. Chem. **37**, 1680 (1959).
[63]K. Furukawa and E. A. Ogryzlo, Chem. Phys. Lett. **12**, 370 (1971).
[64]R. G. Derwent and B. A. Thrush, Trans. Faraday Soc. **67**, 2036 (1971).
[65]C. E. Moore, *Atomic Energy Levels* (U.S. GPO, Washington, D.C., 1971), Vol. 35.
[66]R. G. Avilés, D. F. Muller, and P. L. Houston, Appl. Phys. Lett. **37**, 358 (1980).
[67]R. G. Bray and R. M. Hochstrasser, Mol. Phys. **31**, 1199 (1976). In Table 2 of this reference, for *P*-branch lines of a $|\Omega \pm 1\rangle \leftarrow |\Omega\rangle$ electronic transition, the first factor in the numerator should read $(J \mp \Omega - 1)$.
[68]W. M. McClain and R. A. Harris, in *Excited States*, edited by E. C. Lim (Academic, New York, 1977), Vol. III.
[69]F. Metz, W. E. Howard, L. Wunsch, H. J. Neusser, and E. W. Schlag, Proc. R. Soc. London, Ser. A **363**, 381 (1978).
[70]K.-M. Chen and E. S. Yeung, J. Chem. Phys. **69**, 43 (1978).
[71]J. B. Halpern, H. Zacharias, and R. Wallenstein, J. Mol. Spectrosc. **79**, 1 (1980).
[72]C. Maïnos, Y. LeDuff, and E. Boursey, Mol. Phys. **56**, 1165 (1985).
[73]M. A. C. Nascimento, Chem. Phys. **74**, 51 (1983).
[74]G. C. Nieman, J. Chem. Phys. **75**, 584 (1981).
[75]C. Maïnos and Y. LeDuff, Mol. Phys. **60**, 383 (1987).
[76]C. Maïnos, Phys. Rev. A **33**, 3983 (1986).
[77]R. R. Ogorzalek Loo, Ph. D. dissertation, Cornell University, Ithaca, New York, 1989.
[78]R.F. Marks, R. A. Gottscho, and R. W. Field, Phys. Scr. **25**, 312 (1982).
[79]R. W. Field, A. Lagerqvist, and I. Renhorn, Phys. Scr. **14**, 298 (1976).
[80]W. C. Ermler and R. S. Mulliken, J. Mol. Spectrosc. **61**, 100 (1976).
[81]E. A. Colbourn and A. E. Douglas, J. Mol. Spectrosc. **65**, 332 (1977).
[82]G. Herzberg, *Molecular Spectra and Molecular Structure: I. Spectra of Diatomic Molecules* (Van Nostrand, Princeton, NJ, 1950) p. 223.
[83]H. Lefebvre-Brion and R. W. Field, *Perturbations in the Spectra of Diatomic Molecules* (Academic, New York, 1986), pp. 56–57.
[84]G. Herzberg, *Molecular Spectra and Molecular Structure: I. Spectra of Diatomic Molecules* (Van Nostrand, Princeton, NJ, 1950), p. 244.
[85]L. W. Bader and E. A. Ogryzlo, Discuss. Faraday Soc. **37**, 46 (1964).
[86]R. A. Young and G. Black, J. Phys. Chem. **44**, 3741 (1966).
[87]R. F. Heidner III, C. E. Gardner, T. M. El-Sayed, G. I. Segal, and J. V. V. Kasper, J. Chem. Phys. **74**, 5618 (1981).
[88]R. G. Derwent and B. A. Thrush, Faraday Discuss. Chem. Soc. **53**, 162 (1972).
[89]P. M. Borrell, P. Borrell, and K. G. Grant, J. Chem. Phys. **78**, 748 (1983).
[90]B. A. Garetz and C. Kittrell, Phys. Rev. Lett. **53**, 156 (1984).
[91]A. Recknagel, Z. Phys. **87**, 375 (1934).
[92]J. H. van Vleck, Rev. Mod. Phys. **23**, 213 (1951).
[93]L. Veseth, Theor. Chim. Acta **18**, 368 (1970).
[94]K. Kayama and J. C. Baird, J. Chem. Phys. **46**, 2604 (1967).